



AALBORG UNIVERSITET

**Effect of Selection Pressure with Temozolomide on
Cripto-1 Expression in Glioblastoma In Vitro Models**

Cansu Yener

9th and 10th Semester - Master Thesis

Biomedicine, Department of Health and Science & Technology

Aalborg University, Spring 2018

Title: Effect of Selection Pressure with Temozolomide on Cripto-1 Expression in Glioblastoma In Vitro Models

Project group: 9044

Semester: 9th and 10th Semester Master Thesis – Biomedicine, Aalborg University

Project period: September 2017 – May 2018

Author:



Cansu Yener

Supervisor: Linda Pilgaard
Associate Professor

Pages: 42 pages

Appendix: 4 pages

Medicine with Industrial Specialization - Biomedicine
Department of Health Science and Technology
Aalborg University - Frederik Bajers Vej 7 9220 Aalborg Denmark

ABSTRACT

Introduction: Glioblastoma multiforme (GBM) is a stage IV aggressive brain cancer, which has poor prognosis with a median survival of 12-15 months. Conventional treatment approaches consisting of surgical resection and chemo- and radiotherapy offer only palliation expanding the lifetime by a few months. The inevitable regrowth of GBM is thought to be caused by a subpopulation of glioblastoma-initiating cells (GICs), which is characterized by their special migratory properties, stem cell characteristics, and resistance to conventional therapies. The protein Cripto-1 (CR-1) has been correlated to the pathogenesis of cancer and identified as a possible marker for GICs, which can be an attractive target for cancer therapy.

Methods: GBM cell lines U87, T78, and T87 were exposed to a double-cycle treatment with cytostatic temozolomide (TMZ). DMSO-treated cells were used as the vehicle control group. The effect of the TMZ-treatment on GBM cell lines was investigated using functional assays regarding cell viability and proliferation as well as self-renewal ability. Furthermore, the effect of TMZ-treatment on CR-1 expression and its relation to the self-renewal ability of GICs was explored using qPCR and flow cytometric analysis.

Results: U87 cells demonstrated sensitivity to the treatment in regards to viability, proliferation, and self-renewal ability. CR-1 expression showed to decrease upon TMZ-treatment. T78 cells showed a decrease in functional features upon first treatment cycle, where a revival was observed upon second cycle. T87 demonstrated similar features as the control DMSO group while an increase in CR-1 expression was displayed upon second TMZ treatment cycle. DMSO-treatment showed to decrease the cellular proliferation for all three cell lines.

Conclusion: The GBM cell lines responded differently to the TMZ double-cycle treatment, which may be related to their genetic tumor profiles. The features of GICs have not been possible to detect in this study by using CR-1 as a possible marker for GIC population. Further research is therefore needed in order to investigate the effect of TMZ on GBM in vitro models and how the GIC population is affected by therapeutic selection pressure by TMZ.

RESUME

Introduktion: Glioblastoma multiforme (GBM) er en aggressiv hjerne cancer (stadie IV), som har en dårlig prognose med en median overlevelse på 12-15 måneder. Konventionelle behandlingsmetoder, som består af kirurgisk resektion samt kemo- og radioterapi, tilbyder kun palliation, der forlænger livstiden med nogle få måneder. Den uundgåelige fornyede vækst af GBM menes at være forårsaget af en subpopulation betegnet glioblastoma-initierende celler (GICs), som har vist migrerende egenskaber, stamcellekarakteristika samt resistens for konventionelle behandlinger. Proteinet Cripto-1 (CR-1) associeres med patogenesen af cancer og er blevet identificeret som en mulig markør for GICs, hvilket kan være et attraktivt mål for cancerbehandling.

Metoder: GBM cellelinjerne U87, T78 og T87 har været udsat for en dobbeltcyklus behandling med cytostatisk temozolomid (TMZ). DMSO behandlede celler er blevet anvendt som kontrolgruppe. Effekten af TMZ-behandlingen på GBM cellelinjerne er blevet undersøgt ved anvendelse af funktionelle analyser vedrørende cellelevedygtigheden og proliferation samt selvfornyelsesevne. Endvidere blev effekten af TMZ-behandlingen på CR-1 ekspressionen og dens relation til selvfornyelsesevnen af GICs udforsket ved anvendelsen af metoder som qPCR og flowcytometri.

Resultater: U87 celler viste sensitivitet overfor TMZ-behandlingen, hvor der var tale om nedsat levedygtighed, proliferation og selvfornyelsesevne. CR-1 ekspressionen viste et fald ved TMZ-behandling. T78 cellerne viste reduceret funktionelle egenskaber ved første TMZ-behandling, hvor genoplivning blev observeret i andet cyklus. T87 demonstrerede lignende træk som DMSO-kontrolgruppen, mens en stigning i CR-1 ekspressionen blev observeret ved anden TMZ-behandling. Yderligere viste DMSO-behandling at reducere den cellulære proliferation i alle tre GBM cellelinjer.

Konklusion: De tre GBM cellelinjer reagerede forskelligt på TMZ dobbeltcyklusbehandlingen, hvilket kan skyldes deres genetiske tumorprofiler. Resultaterne vedrørende CR-1 udtrykkelsen og dets relation til GICs har ikke været afklarende i dette studie. Yderligere undersøgelser er derfor nødvendige for at undersøge effekten af TMZ på GBM in vitro modeller og hvordan GICs påvirkes af terapeutisk selektionspres med TMZ.

ABBREVIATIONS

bFGF:	Basic Fibroblast Growth Factor
CFSE:	Carboxyfluorescein Succinimidyl Ester
CFU:	Colony-Forming Unit
CR-1:	Human Cripto-1
EGFR	Epidermal Growth Factor Receptor
DMSO:	Dimethylsulfoxid
EC	Human Embryonal Carcinoma
EGF:	Epidermal Growth Factor
EMT:	Epithelial-Mesenchymal Transition
GBM:	Glioblastoma Multiforme
GICs:	Glioblastoma-Initiating Cells
GPI:	Glycosylphosphatidylinositol
IDH1:	Isocitrate Dehydrogenase
MFI	Mean Fluorescence Intensity
MGMT:	Methylguanine-DNA Methyltransferase
MTIC	5-(3-methyltriazene-1-yl) imidazole-4-carboxamide
TICs:	Tumor-Initiating Cells
TGF- β :	Transforming Growth factor- β
TMZ:	Temozolomide

TABLE OF CONTENTS

1 – INTRODUCTION	7
1.1 – GLIOBLASTOMA MULTIFORME.....	7
1.2 – TEMOZOLOMIDE	8
1.3 – GLIOBLASTOMA-INITIATING CELLS AND THE CHEMORESISTANCE THEORY.....	9
1.4 – HUMAN CRIPTO-1.....	10
1.4.1 ROLE OF CRIPTO-1 IN EMBRYONIC DEVELOPMENT	11
1.4.2 ROLE OF CRIPTO-1 IN ONCOGENIC TRANSFORMATION	12
1.4.3 CRIPTO-1 AS A MARKER FOR GLIOBLASTOMA-INITIATING CELLS	13
2 – PURPOSE OF THE STUDY.....	14
3 – MATERIALS AND METHODS	15
3.1 – GBM CELL LINES.....	15
3.2 – CELL CULTURE AND TEMOZOLOMIDE TREATMENT	15
3.3 – GENERATION OF PROLIFERATION CURVES	16
3.4 – COLONY-FORMING UNIT ASSAY.....	16
3.5 – DETECTION OF TRANSCRIPTIONAL ACTIVITY	17
3.6 – DETECTION OF CELL PROLIFERATION AND CR-1 EXPRESSION.....	18
3.6.1 – CFSE CELL PROLIFERATION TRACKING	18
3.6.2 – DETECTION OF CR-1 EXPRESSION	19
3.7 – STATISTICAL ANALYSIS	19
4 – RESULTS.....	20
4.1 – MORPHOLOGICAL ANALYSIS OF PRIMARY AND MODEL GBM CELL LINES EXPOSED TO TMZ DOUBLE-CYCLE TREATMENT.....	20
4.2 – CELL VIABILITY AND PROLIFERATION FOLLOWING TMZ DOUBLE-CYCLE TREATMENT	22
4.3 – COLONY-FORMING ABILITY OF GBM CELL LINES.....	26
4.4 – TRANSCRIPTIONAL ACTIVITY OF THE GENES CCND2, GADD45G, AND CRIPTO-1 AFTER TMZ DOUBLE-CYCLE TREATMENT.....	28
4.5 – CELL PROLIFERATION TRACKING AND CRIPTO-1 EXPRESSION AFTER TMZ-TREATMENT	30
5 – DISCUSSION	32
6 – CONCLUSION	36
7 – FUTURE APPLICATIONS	37
BIBLIOGRAPHY.....	38
APPENDIX.....	43
APPENDIX 1 – COLONY-FORMING UNIT (CFU) ASSAY PLATE SETUP	43
APPENDIX 2 – QPCR DATA OUTPUT	44
APPENDIX 3 – FLOW CYTOMETRY DATA OUTPUT.....	46

1 – INTRODUCTION

1.1 – GLIOBLASTOMA MULTIFORME

Glioblastoma multiforme (GBM) is a stage IV aggressive brain cancer, which is the most common malignant brain tumor of the central nervous system (CNS) (1). GBM accounts for approximately 60% of all brain tumors with a median age of 64 and a higher incidence for men (2,3). The prognosis for GBM is poor with a median survival of 12-15 months. Less than 5% of the patients survive within 5 years (4).

GBM is characterized by infiltrating surrounding brain tissues leading to tumor growth and extensive tumor vascularization. Additional GBM characteristics are the presence of necrotic regions surrounded by palisading cells. The grading of GBM is based on pathological features, which include mitotic activity, nuclear atypia, vascular proliferation, necrosis, and proliferation potential as well as clinical and treatment outcomes. (3,5) GBM is further categorized into clinical and molecular subtypes. Clinical subtypes comprise primary and secondary GBM, where the most common type is primary subtype, which accounts for approximately 95% of GBM cases. It develops *de novo* in older patients within 3-6 months. In contrast to the primary subtype, secondary GBM is seen dominantly in younger patients and develops over 10-15 years from prior low-grade astrocytomas. The two groups demonstrate certain differences in gene expressions; however, the outcome is similar as the affected signaling pathways for both subtypes result in abnormal regulation of cellular systems including cell cycle and growth factor mediated signaling pathways. (3,6)

The Cancer Genome Atlas (TCGA) has described a gene expression-based molecular classification, which comprises the classical, mesenchymal, proneural, and neural subtype (7,8). Tabel 1.1 demonstrates a detailed overview of the common alterations for the four GBM subtypes. The classical subtype is described to express atypically high levels of epidermal growth factor receptor (EGFR), which is a protein functioning in cell growth. Occurrence of the abnormality in EGFR levels is lower in the other GBM subtypes. The mesenchymal subtype is associated with the most frequent numbers of mutations in the tumor suppressor gene NF1 as well as mutation in the tumor suppressor genes PTEN and TP53. Proneural tumors are characterized by the most frequent mutations in the isocitrate dehydrogenase 1 (IDH1) gene, which contributes to abnormal cell growth, as well as a significant mutation in the tumor suppressor gene TP53. Neural GBM subgroup contains mutations in the same genes as listed above. (7) Genes involved in the classical and mesenchymal subtype have shown correlation to shorter overall survival time compared to the other subtypes (9). Furthermore, GBM patients belonging to the mesenchymal profile is associated with epithelial-mesenchymal transition (EMT) due to high tumor invasiveness (10,11). The subtype has

also showed to express mesenchymal markers as CHI3L1 and MET (Table 1.1). EMT is further described in later sections. The subtypes have demonstrated different responses to the treatments, however, the clinical significance of the GBM subtypes still remains unclear (12).

Table 1.1 Characteristic alterations in GBM subtypes (7)

Subtype	Characteristic alterations	Survival
Classical	↑ EGFR, Nestin, NOTCH3, JAG1, and LFNG ↓ CDKN2A	Poor
Mesenchymal	Mutated NFI, PTEN, and p53 ↑ CHI3L1 (also known as YKL40), MET, CD44, and MERTK	Poor
Proneural	Mutated IDH1 and TP53 ↑ PDGFRA, OLIG2, TCF-3, DCX, and DLL3	Better
Neural	↑ Neuronal markers such as NEFL, GABRA1, SYT1, and SLC12A5	Poor

Current treatment approaches for GBM patients include maximal safe surgical resection followed by combined radio- and chemotherapy treatment. However, these approaches offer only palliation extending the lifespan of patients by few months (13). Maximal surgical resection relieves the tumor-associated symptoms and gives a confirmation of the diagnosis pathologically (14,15). The chemotherapy treatment of first choice for newly diagnosed GBM is the alkylating agent temozolomide (13,16).

1.2 - TEMOZOLOMIDE

Temozolomide (Temodar®, Temodal®, TMZ) is an orally administered monofunctional alkylating agent, which is approved for use in treatment of newly diagnosed adult GBM in 2005. Due to the lipophilic properties, it has the ability to cross the blood-brain barrier. (17,18)

Recommended treatment schedule for newly diagnosed GBM patients includes a daily dose of 75 mg/m² for 42 days concomitantly with radiotherapy. This treatment is followed by six weeks of treatment cycles, where the patients daily are given 150 mg/m² of TMZ for consecutive 5 days followed by a rest period with no treatment for 23 days prior to next treatment cycle. Intravenous administration is also possible, where TMZ is injected over 90 minutes with the same dose administered orally. (17,19) The common side effects of TMZ

are among others fatigue, headache, nausea, vomiting, hair loss, anaemia, loss of appetite, viral infection, and insomnia (20).

TMZ is stable at acidic pH (<5), but in case of neutral and alkaline pH (>7) it is rapidly hydrolysed to 5-(3-methyltriazene-1-yl) imidazole-4-carboxamide (MTIC) (17,18). The reaction of MTIC with water leads to the release of 5-aminoimidazole-4-carboxamide (AIC) and the reactive methyldiazonium cation. Methyldiazonium cation methylates DNA at N⁷ and O⁶ positions of guanine (N⁷-MeG and O⁶-MeG) and O³ of adenine (O³-MeA), which elicit the cytotoxicity of TMZ. O⁶-MeG induces cell death through double-strand breaks and base mispairing. However, a direct repair mechanism for this lesion is present. (16) O⁶-MeG can be directly repaired by the enzyme methylguanine-DNA methyltransferase (MGMT), which is able to remove the methyl adduct and thereby repair the TMZ-induced DNA damage (4,21). Consequently, the intracellular level of MGMT is associated with chemoresistance. Methylation of the MGMT gene promoter is seen in about 50% of GBM, which results in silencing of the enzyme and thereby increases the sensitivity to TMZ treatment. (21,22)

1.3- GLIOBLASTOMA-INITIATING CELLS AND THE CHEMO-RESISTANCE THEORY

An additional chemoresistance theory is based on a subpopulation designated tumor-initiating cells (TICs). The ability of GBM cells to escape chemo- and radiotherapy leading to inevitable tumor regrowth is mainly believed to be caused by the small subpopulation TICs. This subpopulation has demonstrated stem cell characteristics, which implies maintained proliferation, self-renewal and differentiation ability as well as resistance to chemo- and radiotherapy (23). TICs have been identified in the hematopoietic system as well as in solid tumors including those arising from the brain, lung, breast, colon, head and neck, and pancreas (24). TICs isolated from GBM are also known as glioblastoma-initiating cells (GICs) and are found to be located in hypoxic areas of GBM.

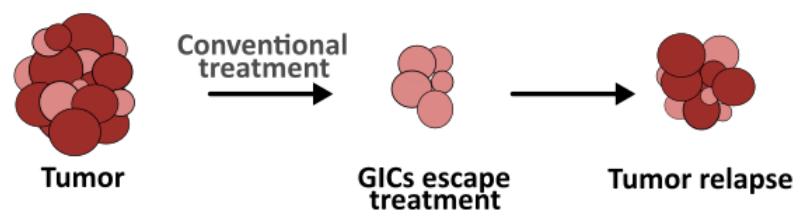


Figure 1.1 Chemoresistance theory of GICs. GBM is composed of a heterogeneous group of cancer cells. Glioblastoma-initiating cells (GICs) is a subpopulation, which have shown stem cell characteristics as maintained proliferation, self-renewal ability, and resistance to conventional therapy. GICs are suggested to be responsible for regrowth following conventional therapy.

The origin of GICs still remains unclear, however, the speculations are centered on three theories. One hypothesis is based on the dedifferentiation of mature glia cells upon mutations, which lead to acquisition of stem-like properties. The other two theories are centered on neural progenitors and adult neural stem cells, which upon mutation will acquire unregulated stem-like features. (25) GICs are considered to be quiescent in the tumor, which lead to the suggestion of GICs being resistance to chemo- and radiotherapy, as the main target for the conventional therapy is rapidly dividing cells (26). GICs will therefore survive anticancer treatments and lead to tumor recurrence (Figure 1.1). Evidence has suggested that GIC chemoresistance and tumor recurrence among others are mediated through several mechanisms including alterations in DNA-damage responses and cell cycle regulation (27,28).

Evidence reveals that GICs express cell-surface markers, which are also expressed by normal stem cells. One of the first studies about GICs was performed by Singh *et al*, which identified the GIC population by the marker prominin-1 (CD133). The study demonstrated that CD133-positive cells were able to recapitulate the phenotype of the initial tumor (29). However, the reliability of CD133 as a GIC marker remains questionable, as recent studies have shown that CD133-negative cells also have tumorigenic potential (30,31). GICs have among others also been found to express the stem cell markers nestin and Sox2 (25). Recent investigations have also identified the embryonic gene Cripto-1 as a marker for GICs, which may be a new field of interest as a therapeutic target in GBM (32,33).

1.4 – HUMAN CRIPTO-1

Human Cripto-1 (CR-1), also known as teratocarcinoma-derived growth factor, is a glycoprotein belonging to the epidermal growth factor (EGF)-cripto-1-FRL-1-cryptic (CFC) gene family. It is found in low expression levels in different adult tissues and organs, where the highest CR-1 expression is found in the cortex of adrenal gland and colon. CR-1 is known to participate in processes involving stem cell maintenance, cell proliferation, migration, and angiogenesis (34). High expression levels of CR-1 are detected in several human carcinomas including breast, lung, colon, pancreas, and ovary (24).

The structure of CR-1 consists of an NH₂-terminal signal sequence for extracellular secretion, a modified EGF-like domain, a conserved cysteine-rich domain (CFC-motif), and a short hydrophobic carboxy-terminus, containing sequences for glycosylphosphatidylinositol (GPI). GPI functions as an anchor attached to the cell membrane. The GPI anchor can be removed by GPI-phospholipase D (GPI-PLD), which leads to the generation of a soluble biologically active CR-1. Cell membrane-attached and soluble CR-1 is associated with its own ways of reaction pathways. (24)

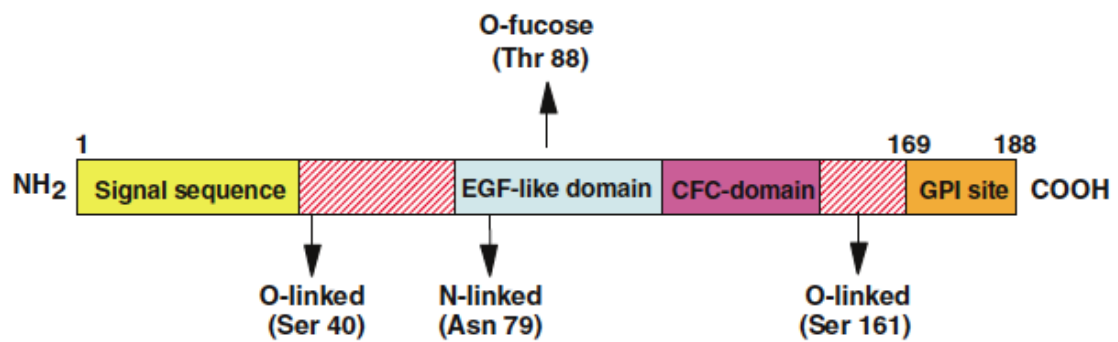


Figure 1.2 Composition of Cripto-1 (CR-1) glycoprotein. CR-1 is composed of an NH₂-terminal signal sequence for extracellular secretion, a modified EGF-like domain, a conserved cysteine-rich domain (CFC-motif), and a short hydrophobic carboxy-terminus, containing sequences for glycosylphosphatidylinositol (GPI). (37)

CR-1 is known to be involved in several signaling pathways; the main CR-1-activated pathways consist of the Nodal/ALK4/ALK7/Smad-2 signaling pathway and the Glypocan-1/c-Src/MAPK/AKT signaling pathway.

1.4.1 ROLE OF CRIPTO-1 IN EMBRYONIC DEVELOPMENT

Cell membrane-attached CR-1 functions as a co-receptor for the transforming growth factor- β (TGF- β)-related peptides Nodal and Growth and differentiation factor 1 and 3 (GDF1 and GDF3). This occurs through a complex composed of type I (ALK4 or ALK7) and type II (ActRII or ActRIIB) Activin serine-threonine kinase receptors. Activation of ALK4 leads to phosphorylation of receptor-regulated proteins Smad-2 and Smad-3, which subsequently bind to Smad-4, also known as the common partner Smad (co-Smad), and form a transcriptional complex. The complex translocates to the nucleus and leads to transcriptional up-regulation of specific target genes. (35,36)

Independently from CR-1, Nodal is able to bind directly to Alk7, while Alk4 signaling is dependent on the interaction with CR-1. CR-1/Nodal signaling pathway is involved in several events during the embryonic development; this includes the formation of the primitive streak, development of the anterior-posterior axis, specification of mesoderm and endoderm during gastrulation, and formation of left-right asymmetry of developing organs. (24)

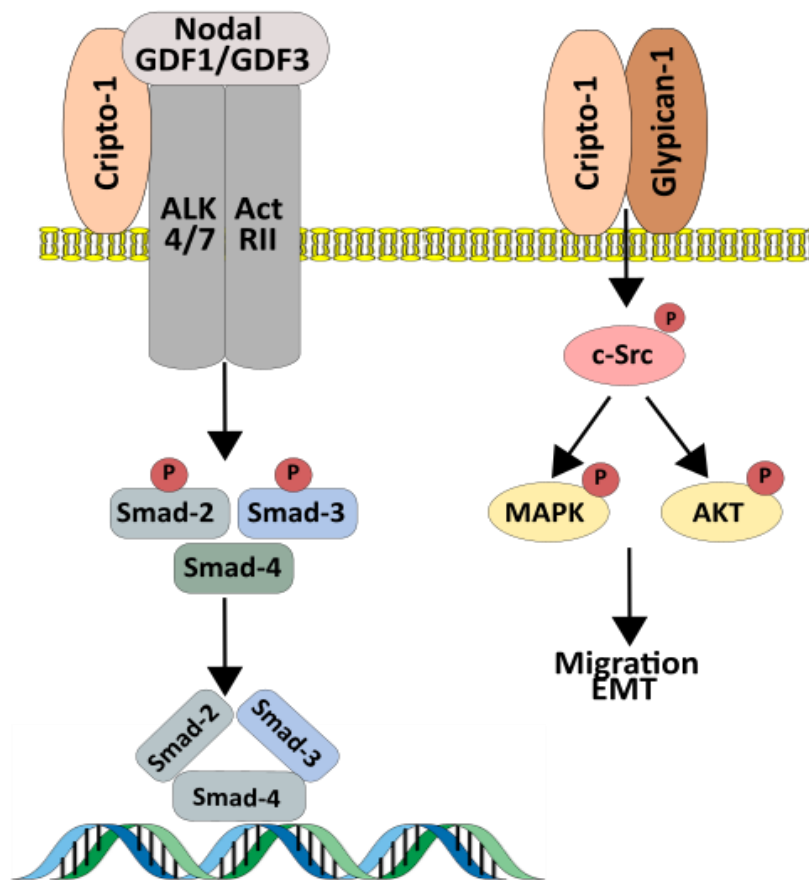


Figure 1.3 CR-1 and its involvement in the Nodal/ALK4/ALK7/Smad-2 signaling pathway and the Glypican-1/c-Src/MAPK/AKT signaling pathway. Adapted from Bianco *et al* (24)

1.4.2 ROLE OF CRIPTO-1 IN ONCOGENIC TRANSFORMATION

Besides functioning as a co-receptor for Nodal/GDF1/GDF3, CR-1 has the ability to bind to Glypican-1, which is a GPI-anchored heparin sulphate proteoglycan (HSPG) (33,35). The binding leads to phosphorylation of cytoplasmic tyrosine kinase c-Src, which results in the activation of mitogen-activated protein kinase (MAPK)/phosphatidylinositol 3'kinase (PI3K)/Protein kinase B (Akt) signalling pathways, which are involved in regulation of cell proliferation, survival, and motility. Due to the activation of these signaling pathways, which occurs independently of Nodal and ALK4, CR-1 is known to participate in the pathogenesis of cancer. (35,37) CR-1 also interacts with the Wnt/ β -catenin signalling pathway, which can lead to the regulation of processes including cell migration and invasion (38).

CR-1 has also demonstrated a significant role in the regulation of EMT (39). EMT is a biological process, where epithelial cells lose their characteristics and acquire invasive and migratory mesenchymal features (40,41). In a study by Strizzi *et al*, Transgenic HC-11

mouse mammary epithelial cells overexpressing CR-1 demonstrated expression alterations in markers, which are known to characterize the EMT process. Expression of E-cadherin, a transmembrane glycoprotein responsible for linking epithelial cells, was significantly decreased, whereas a significant increase in the markers N-cadherin and Vimentin was detected. N-cadherin and Vimentin are mesenchymal markers contributing with transient adhesive properties. (39,42) A study by Ebert *et al* used CR-1 overexpressed human cervical carcinoma cells, which showed an increase in the expression of Vimentin. The same cells demonstrated an increase in migratory and invasive properties, which was observed by using matrix-coated membranes; due to this result, CR-1 was suggested to contribute to the aggressive tumor progression of cervical carcinoma. (34)

1.4.3 CRIPTO-1 AS A MARKER FOR GLIOBLASTOMA-INITIATING CELLS

A study has detected a heterogeneous expression of CR-1 in a subpopulation of TICs in human embryonal carcinoma (EC). The subpopulation was further separated in two groups representing EC cells with high (CR-1^{High}) and low (CR-1^{Low}) CR-1 expression pattern. Results obtained from the segregation demonstrated different gene expressions and tumorigenic capacity. CR-1^{High} generated tumor spheres in serum-free culture conditions more efficiently compared to CR-1^{Low}. Additionally, subcutaneous injection gave rise to larger tumors formed by CR-1^{High} demonstrated in a shorter latency period in contrast to CR-1^{Low}. (32,43) CR-1 positive cells have also been seen in a small subpopulation of cells with stem-like characteristics in human malignant melanoma. Compared to parental melanoma cells, CR-1 positive subpopulation was observed to have an increase in stem cell markers Oct4 and SUZ-14. (43,44)

A study by Tysnes *et al* showed that high CR-1 expression was associated with shorter survival of GBM patients (45). CR-1 has been identified in different areas of GBM tissue, which comprise perivascular tumor cells and endothelial cells. Based on the knowledge that GBM cells grow near blood vessels and thereby form a hypoxic niche as the tumor grows, CR-1 expression may indicate the presence of GICs (46). These findings support that CR-1 is a possible marker for GICs and that this could be a candidate target for cancer therapy

2 – PURPOSE OF THE STUDY

In this study, the effect of selection pressure with the cytostatic TMZ on GBM in vitro models will be investigated regarding functional features. Furthermore, the effect of TMZ treatments on the expression level of CR-1 and its relation to the self-renewal capabilities of GICs will be explored.

For this purpose, the GBM cell lines U87, T78, and T87 will be cultured as neurospheres and exposed to TMZ double-cycle treatment in order to mimic the therapy, which the patients receive in the clinic. DMSO-treated cells will be used as the vehicle control. Following the cycle treatments, the GBM cell lines will be characterized using functional assays regarding cell viability and proliferation, and self-renewal ability. Additionally, the effect of the TMZ double-cycle treatment on cell proliferation, DNA repair mechanisms, and CR-1 expression will be investigated using quantitative methods.

3 – MATERIALS AND METHODS

3.1 – GBM CELL LINES

The cell lines used in this study consisted of the model GBM cell line U87 and the two primary GBM cell lines T78 and T87. U87 cell line is commonly used in GBM research and derives from grade IV GBM obtained from a 44 year-old female patient. The cell lines T78 and T87 are newly established in Odense and obtained from primary GBM tissue (47). Characterization of T78 and T87 reveals that T78 belong to the mesenchymal GBM subtype, whereas T87 belongs to the proneural subtype. Both cell lines are reported to have a methylated MGMT promoter (48). Three other cell lines were used as positive controls as they were known to express CR-1. The cell lines included U87 overexpressing CR-1, which is generated at Aalborg University, NTERA2/D1 deriving from EC, and T10, which is a primary cell line acquired from Danish Cancer Society.

3.2 - CELL CULTURE AND TEMOZOLOMIDE TREATMENT

The cell lines were cultured in serum-free medium as neurospheres, which consisted of Neurobasal Medium (Gibco), 1% B27 supplement (50X; Gibco), 1% 200 mM L-glutamine, 1% Penicillin/Streptomycin (Gibco), 20 ng/mL EGF (Sigma), and bFGF (Peprotech). The cells were incubated in a humidified atmosphere at 37°C containing 20% O₂ and 5% CO₂. The cells were passaged before necrosis developed in the spheres. The cells were exposed to treatment with the cytostatic TMZ (Sigma-Aldrich) in a concentration of 50 µmol/L; the treatment comprised a double-cycle, where one cycle consisted of three days treatment with TMZ followed by three days rest period without treatment (Figure 3.1). Dimethylsulfoxid (DMSO; Sigma-Aldrich) treated cells were used as the control group. The cells were seeded in culture flasks (CellStar; Greiner Bio-One) with a seeding density of 20.000 cells/mL and grown for four days prior to treatment.

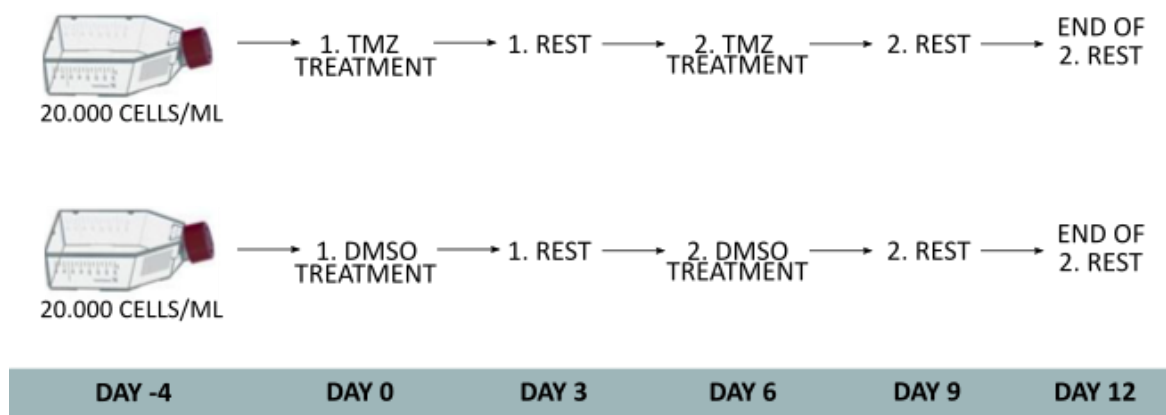


Figure 3.1 Overview of TMZ double-cycle treatment for one cell line, where DMSO-treatment was used as vehicle control group

Phase-contrast images were captured prior to treatment and during the double-cycle treatment. The images were acquired using phase-contrast microscopy 4x objective (PrimoVert; Zeiss) and analysed using the software ImageJ. On figure 3.1, an overview of the double-cycle treatment for one cell line can be seen; this was the fundamental setup used for further analysis, which is described in the following sections.

3.3 - GENERATION OF PROLIFERATION CURVES

In order to detect the effect of the TMZ treatment cycles on cell viability and growth, viability and proliferation curves were generated using the cell counting method. Viability and proliferation curves were generated after each ended rest period. Following dissociation of the neurospheres, the cells were seeded in five 6-well plates (Costar; Corning) as triplicates with appropriate medium in a seeding density of 50.000 cells/well (~ 5000 cells/cm²). Cell viability was assessed by staining with trypan blue (Gibco). Counting was performed using a haemocytometer (Bürker-Türk), where the cells were counted for five consecutive days. Data was plotted in the software GraphPad Prism 7 and thereby an exponential graph was obtained for the proliferation curves. The estimated curves were used for the determination of the doubling times.

3.4 – COLONY-FORMING UNIT ASSAY

Colony-forming unit (CFU) assay was performed to investigate the self-renewal ability and colony formation of the cells after exposing to the treatment cycles. The assay was performed after each ended rest period. After breaking the neurospheres, the cells were counted and resuspended at a concentration of 500 cells/mL. A 2-fold dilution was performed and the cells were seeded in 96-well plates (Costar; Corning) accordingly to appendix 1. The cells were cultured for 10 day and afterwards the fractions of wells without colony formation for each dilution series were estimated. The number of colony-forming units (CFUs) per well was calculated using Poisson distribution. The equation used for the calculation was as follows: $u = -\ln(F_0)$ where F_0 is the fraction of empty wells.

3.5 – DETECTION OF TRANSCRIPTIONAL ACTIVITY

Alterations in transcriptional activity after TMZ double-cycle treatment were investigated using real-time quantitative PCR (qPCR). Transcriptional levels of the genes Cyclin D2 (CCND2), Growth arrest and DNA-damage inducible gene (GADD45G), and CR-1 were investigated. CCND2 functions as a cell-cycle regulator controlling G1 phase progression; the gene is known to be overexpressed in many cancer types (49). The gene GADD45G is detected to increase due to treatment with DNA damaging agents leading to cell cycle arrest and apoptosis (50). YWHAZ was used as the housekeeping gene.

Cells from T25 flasks were lysed with a lysis solution containing 1% β -mercaptoethanol (Bio-rad) and 70% ethanol. RNA harvesting was performed using Aurum Total RNA mini kit (Bio-Rad) according to manufacturers instructions. Quantification of RNA concentration and purity was measured using a spectrophotometer (Nanodrop ND-1000). cDNA synthesis were performed according to manufactures instructions (Bio-Rad) with 1 μ g total RNA input. The samples were run in a thermal cycler (Prime) using the thermal program: 5 min at 25°C, 30 min at 42°C and 5 min at 85°C.

qPCR was performed using a reaction mix containing SYBR Green PCR Master Mix (Applied Biosystems), milli-Q water, forward and reverse primer, and samples diluted in 1:50 (1:200 for two samples). Samples and no template controls (NTC) were loaded into 96-well pcr plates (AriaMx, Agilent Technologies) as duplicates. AriaMx Real-Time PCR system (Agilent Technologies) was used to run the PCR. The qPCR data was further analysed using the software AriaMX and the fold changes were calculated using the Pfaffl-method.

The thermal profile was as the following settings - 1x: 95°C for 5 min (initial activation step); 40x: 95°C for 30 sec, 55°C (CR-1) - 60°C (GADD45G and YWHAZ) - 63°C (CCND2) for 30 sec, 72°C for 30 sec.

Table 3.1 Overview of the primer sequences used for qPCR

	Forward Primer	Reverse Primer
CCND2	TGGTATCTGGCGTTCTTTGG	TGTCTGAGGAATGTTGTGATGG
GADD45G	CAATGTGACCTTCTGTGTGC	CCTGGATCAGCGTAAATGG
CR-1	GATACAGCACAGTAAGGAGC	TAGTTCTGGAGTCCTGGAAG
YWHAZ	ACGCTGGGGTCCTTTGTGCC T	GGGCACAGACCCACAGTTCTCTTT

3.6 – DETECTION OF CELL PROLIFERATION AND CR-1 EXPRESSION

In order to investigate the effect of TMZ double-cycle treatment on cell proliferation and CR-1 expression, flow cytometric analysis was performed.

3.6.1 – CFSE CELL PROLIFERATION TRACKING

Cell proliferation was detected using CellTrace™ CFSE cell Proliferation Kit (Molecular Probes, Life Technologies, Denmark) containing the fluorescent cell staining dye carboxyfluorescein succinimidyl ester (CFSE). The CFSE precursor, carboxyfluorescein diacetate succinimidyl ester (CFDA-SE), is able to passively diffuse into cells where the acetate group will be cleaved by intracellular esterases; this will lead to fluorescent CFSE. CFSE labeling is inherited by cells through cell divisions where the fluorescence intensity will be half of the parent cell.

In this study, CFSE was diluted in PBS in a concentration of 10 μ M and used the same day. The neurospheres were separated to single cells before CFSE use to ensure uniform labeling. Initially, cells were incubated in PBS+CFSE for 15 minutes at 37°C followed by centrifugation. A second incubation was performed for 30 minutes at 37°C where the CFSE underwent acetate hydrolysis. The cells were fixed in 3.7% formaldehyde (Merck) and resuspended in cold PBS before flow cytometry analysis. The samples were run using the flow cytometer CytoFLEX S (Bechman Coulter) and analysed with the software FlowJo (Version 10.4.2).

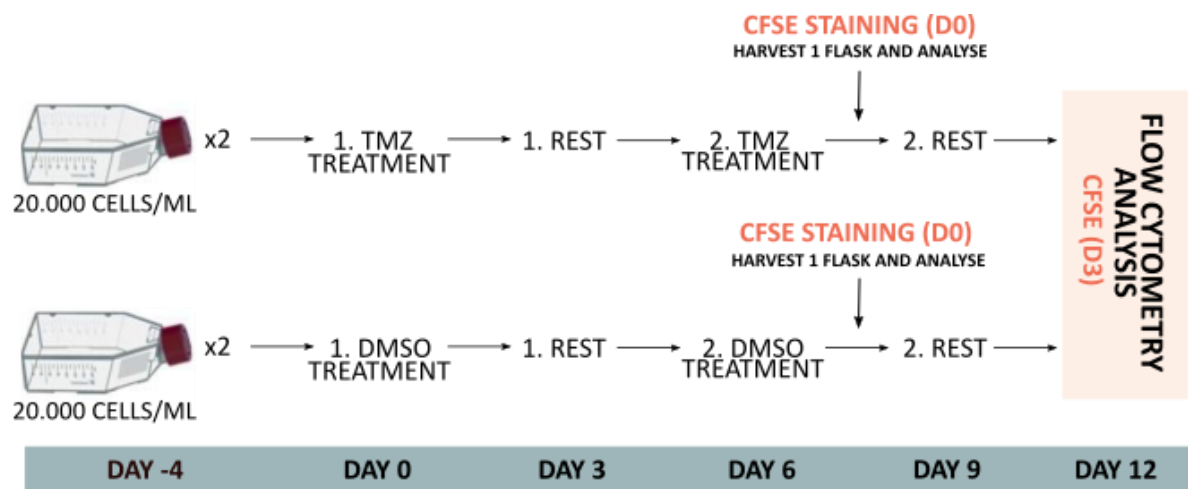


FIGURE 3.3 Experimental setup for CFSE-staining. CFSE-staining was performed after end second treatments for all flasks. This is designated CFSE D0, where harvesting and analysis of undifferentiated CFSE-labelled cells took place. One flask from both treatment and control group with CFSE-labelled cells went through the second rest period and was afterwards harvested and analysed. This was designated CFSE D3.

3.6.2 – DETECTION OF CR-1 EXPRESSION

CR-1 expression of cells exposed to TMZ double-cycle treatment was detected by performing a double staining on cells stained with CFSE. Staining took place at the end of the second rest period. The cells were transferred to falcon tubes and washed twice in PBS. Afterwards, they were treated with tryPLE in order to get single cell suspensions. Before staining, the cells were fixed in 3.7% formaldehyde and resuspended in PBS. The cells were transferred to FACS clear polystyrene tubes (BD Falcon) and the antibodies PE-conjugated mouse monoclonal anti-human Cripto-1 (Cat#FAB2772P, R&D Systems) and PE Mouse IgG1, κ isotype control (BD 555749, BD Biosciences) were added. The cells were incubated for 30-45 min in dark at 4°C and subsequently washed twice in PBS. The samples were run using the flow cytometer CytoFLEX S (Bechman Coulter) and analysed with the software FlowJo (Version 10.4.2).

3.7 – STATISTICAL ANALYSIS

Statistical analysis was performed on PCR results as well as viability and proliferation curves, where the standard error of the mean (SEM) for all measurements was calculated. The calculations were performed using Microsoft Excel and GraphPad Prism 7. Furthermore, statistical significant differences were calculated using t-test analysis in Microsoft Excel and One-way ANOVA in the software SPSS (Version 23). Statistical significance level was set to 0,05.

4 – RESULTS

4.1- MORPHOLOGICAL ANALYSIS OF PRIMARY AND MODEL GBM CELL LINES EXPOSED TO TMZ DOUBLE-CYCLE TREATMENT

The morphological changes of GBM cell lines exposed to TMZ double-cycle treatment and the DMSO-treatment were observed using phase-contrast microscopy. Images of untreated cells for the three cell lines were acquired prior to drug treatment. U87 cells grown as neurospheres appeared as non-adherent small clusters without a sharp defined edge (Figure 4.1A) when compared to T78 neurospheres (Figure 4.1B). T78 neurospheres were observed to be larger and more defined compared to the other two cell lines. In contrast to U87 and T78, which were non-adherent, T87 cells formed both spheres and appeared to be adherent to the plastic surface even though it was cultured in serum-free medium (Figure 4.1C).

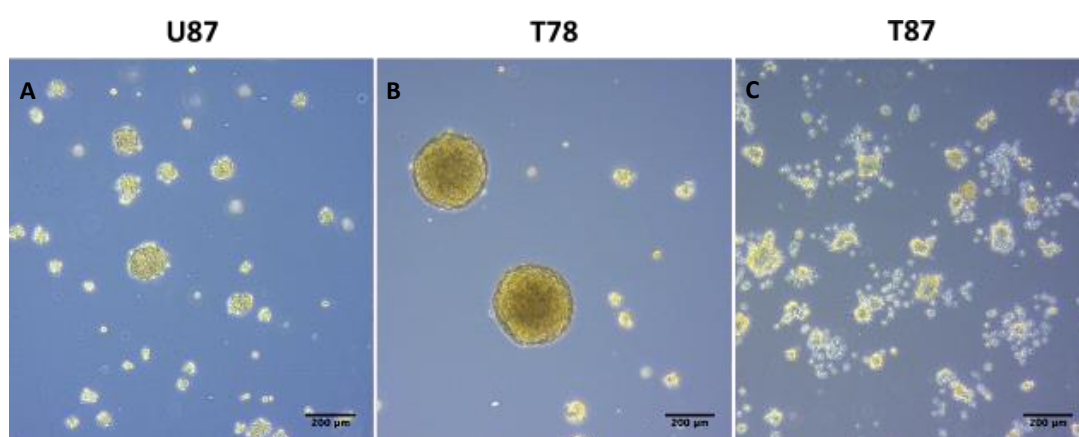


Figure 4.1 Phase-contrast images of untreated GBM cells **A)** U87 neurospheres **B)** T78 neurospheres **C)** T87 neurospheres. Images were taken with 4x magnification. Scale bar, 200 µm

U87 cells exposed to the first TMZ-treatment were observed to contain smaller neurospheres (Figure 4.2A) compared to the control cells, which received first DMSO-treatment (Figure 4.2E). During the first rest period after treatment, it was observed that the cells formed larger spheres but still had small cell clusters (Figure 4.2B) compared to the control cells (Figure 4.2F). After second treatment, the cells preserved the formation of neurospheres although several small cell clusters were present (Figure 4.2C). Following the second rest period, U87 neurospheres were observed to be larger than after the first TMZ-treatment (Figure 4.2D). The control cells, receiving second DMSO-treatment and the final rest period, appeared to attach to the culture flasks both as spheres and cells with a spindle-shaped morphology (Figure 4.2G-H).

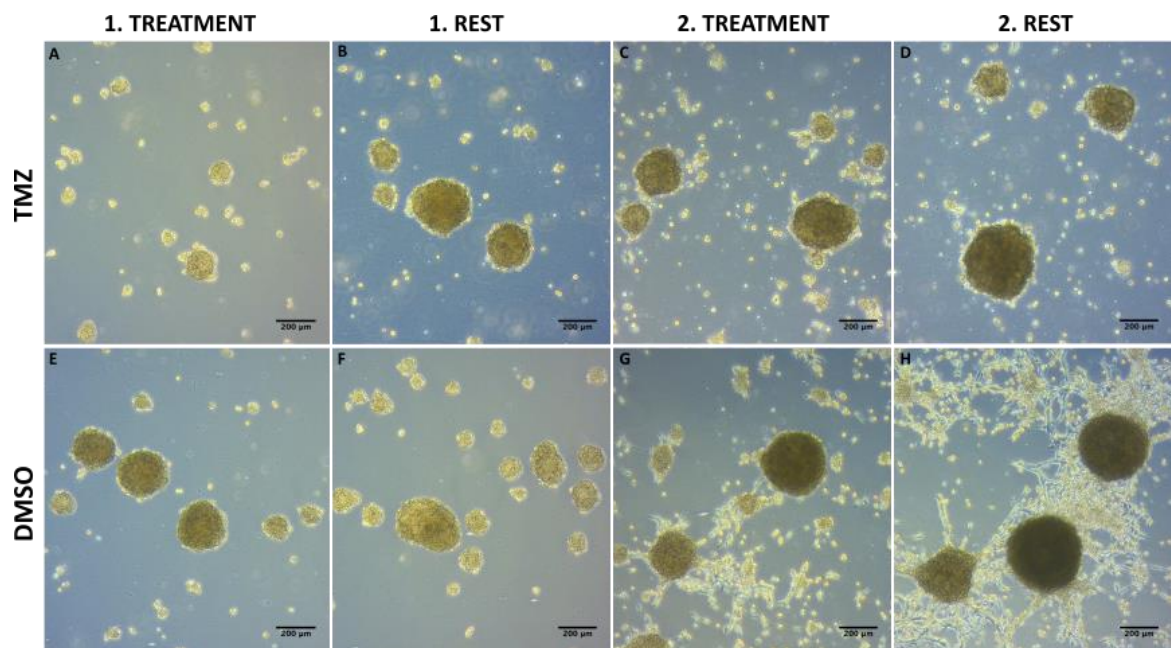


Figure 4.2 Phase-contrast images of U87 cells exposure to TMZ double-cycle treatment and DMSO treatment as vehicle control. **A-D)** U87 cells exposed to TMZ double-cycle treatment **E-H)** U87 cells exposed to DMSO double-cycle treatment. Images were taken with 4x magnification. Scale bar, 200 µm

First TMZ-treatment of T78 cells showed that the sharp defined neurospheres were destroyed into smaller cell clusters as well as clusters, which have lost the circular-shape (Figure 4.3A) compared to the control group (Figure 4.3E). Following the first rest period, the cells obtained the circular neurosphere formation again with the presence of smaller floating cells. After second TMZ-treatment and the rest period, the cells were observed to adhere to the culture flask (Figure 4.3C-D)

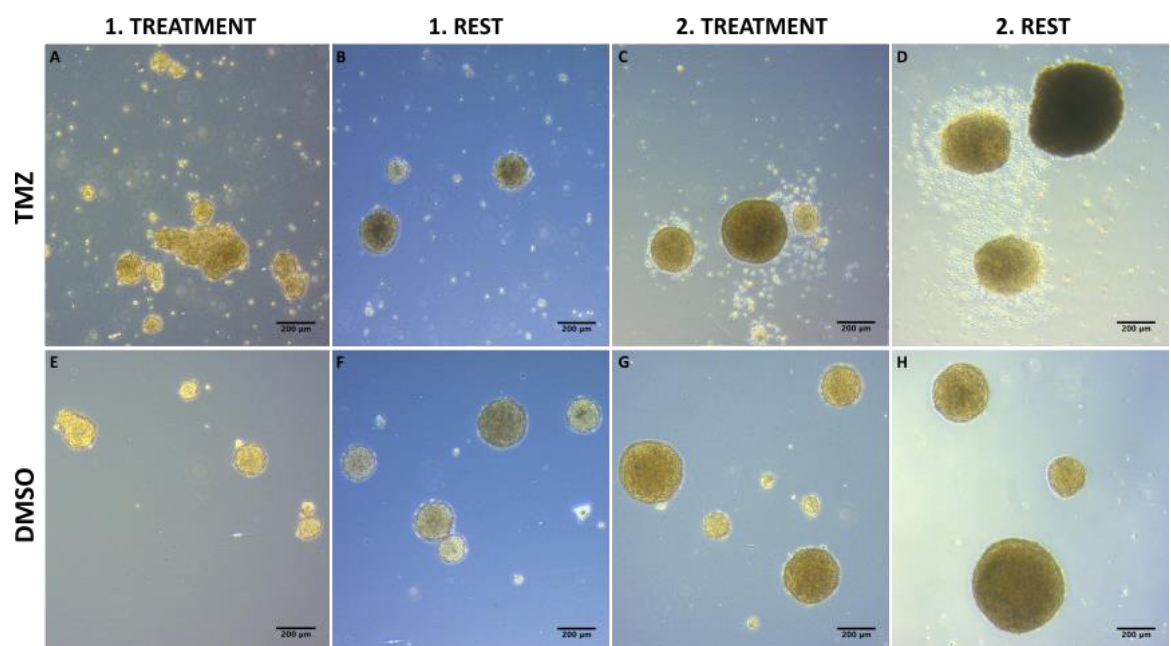


Figure 4.3 Phase-contrast images of T78 cells exposure to TMZ double-cycle treatment and DMSO treatment as vehicle control. **A-D)** T78 cells exposed to TMZ double-cycle treatment **E-H)** T78 cells exposed to DMSO double-cycle treatment. Images were taken with 4x magnification. Scale bar, 200 µm

T87 cells appeared different than the two other cell lines. The double-cycle treatment with TMZ and DMSO demonstrated morphological similarities, which were displayed as adherent cells forming spheres. No difference between the treatment and the control group as well as difference between first and second cycle was observed (Figure 4.4A-H).

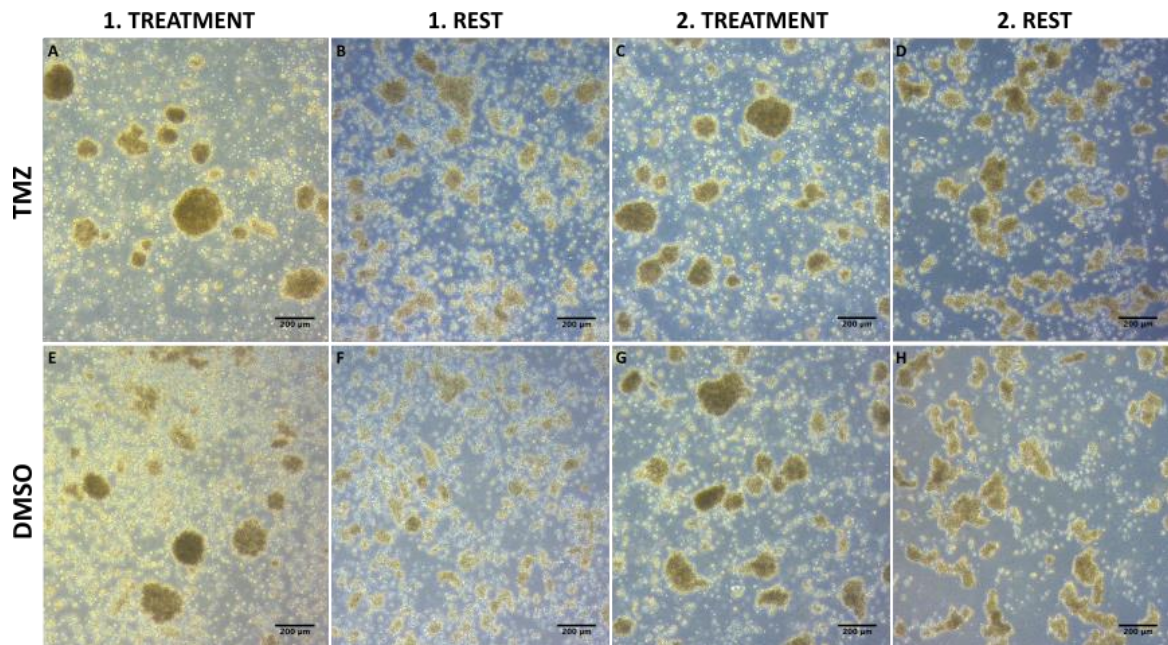


Figure 4.4 Phase-contrast images of T87 cells exposure to TMZ double-cycle treatment and DMSO treatment as vehicle control. **A-D)** T87 cells exposed to TMZ double-cycle treatment **E-H)** T87 cells exposed to DMSO double-cycle treatment. Images were taken with 4x magnification. Scale bar, 200 μ m

4.2 - CELL VIABILITY AND PROLIFERATION FOLLOWING TMZ DOUBLE-CYCLE TREATMENT

To investigate the health and proliferation of the cells following TMZ double-cycle treatment, viability and proliferation curves were acquired after each rest period.

U87 cells exposed to TMZ-treatments demonstrated a decreased viability compared to untreated cells and the DMSO group. After receiving first TMZ-treatment, the cells showed a lower viability compared to untreated cells and the DMSO treatments while the second TMZ-treatment showed the lowest viability, which was observed to increase after day 2. Furthermore, the viability of untreated cells and cells that received first DMSO-treatment appeared similar; the second DMSO-treatment showed to decrease in the beginning and afterwards started to increase. (Figure 4.5A)

The viability of first and second TMZ-treatment of T78 cells was observed to differ from each other. At day 1, cells receiving first TMZ-treatment showed a viability of 40% where a decrease was observed at day 2. At Day 3-4, the curve showed to ascend where a minor decrease was observed at day 5. Second TMZ-treatment presented a viability of approximately 66% at day 1, which was almost similar to day 1 for the first and second DMSO-treated cells. Furthermore, an ascending curve was observed for day 2 and 3 whereas a decrease was seen at day 4, which ended with a minor increase at day 5. A difference between the viability of untreated and DMSO-treated cells was observed as untreated cells showed a higher viability compared to cells receiving both first and second DMSO-treatment. (Figure 4.6A)

First TMZ-treatment for T87 cells showed viability similar to first DMSO-treatment at day 1, following a decrease and an increase at day 2 and 3, respectively (Figure 4.7A). Day 4 and 5 showed a further decrease. At day 1, second TMZ-treatment demonstrated the lowest viability, which was approximately 58%. After the first day, the viability was increased to a level close to the viability of cells, which received the first DMSO-treatment and the second. Second DMSO-treatment started with a viability of nearly 65% and showed an increase in the following four days. Untreated cells demonstrated the highest viability for all five days. (Figure 4.7A)

U87

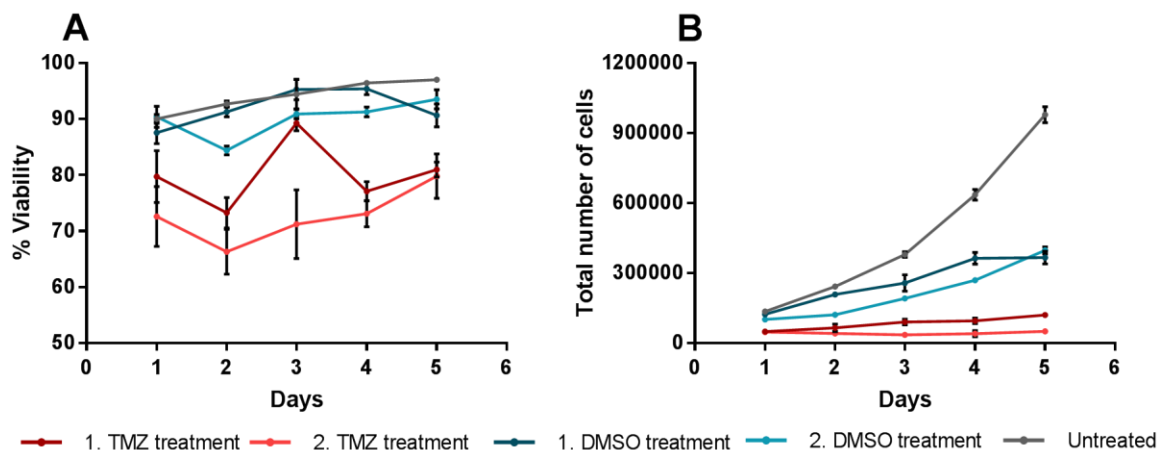


Figure 4.5 Viability and proliferation curves of U87 cell line exposed to TMZ double-cycle treatment and DMSO treatments as the control group. **A)** % Viability of the cells measured for five consecutive days **B)** Proliferation curves assessed from cell counting for consecutive five days. All measurements were obtained from triplicate samples. Error bars for both graphs display the standard error of the mean (SEM)

T78

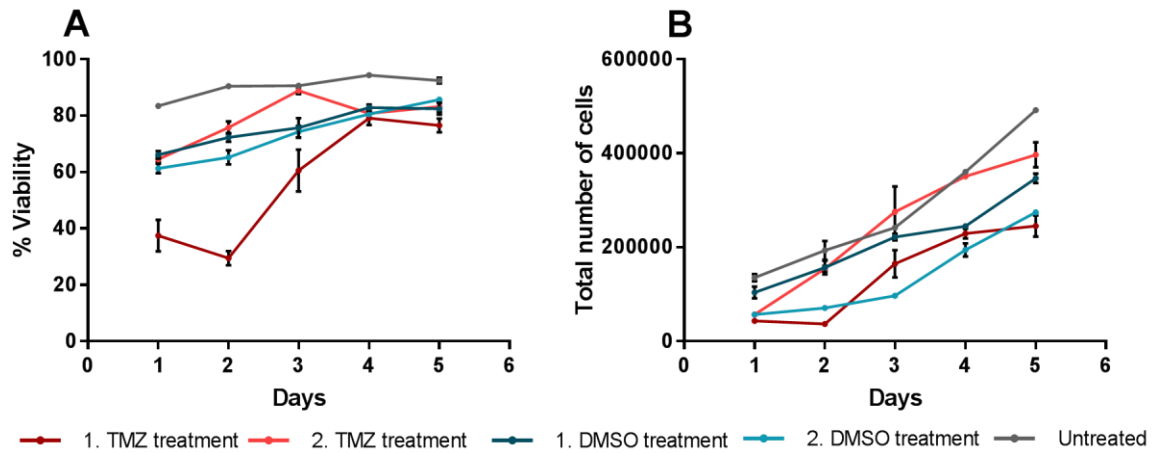


Figure 4.6 Viability and proliferation curves of T78 cell line exposed to TMZ double-cycle treatment and DMSO treatments as the control group. **A)** % Viability of the cells measured for five consecutive days **B)** Proliferation curves assessed from cell counting for consecutive five days. All measurements were obtained from triplicate samples. Error bars for both graphs display the standard error of the mean (SEM)

T87

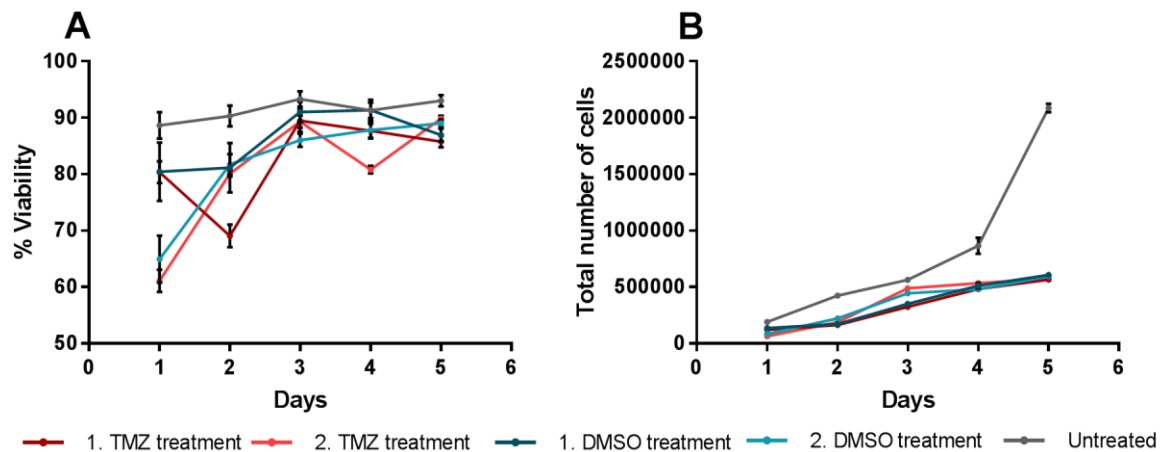


Figure 4.7 Viability and proliferation curves of T87 cell line exposed to TMZ double-cycle treatment and DMSO treatments as the control group. **A)** % Viability of the cells measured for five consecutive days **B)** Proliferation curves assessed from cell counting for consecutive five days. All measurements were obtained from triplicate samples. Error bars for both graphs display the standard error of the mean (SEM)

Proliferation curves for TMZ-treated U87 cells demonstrated an almost straight curve compared to untreated and DMSO-treated cells. A minor increase was seen for the cells after the first TMZ-treatment whereas no proliferation was detected for cells after second TMZ-treatment (Figure 4.5B). The doubling time was calculated to be 3.21 days and 72.96 days for first and second TMZ-treatment, respectively, which was slower compared to the DMSO-treated cells (Figure 4.8A). Both first and second DMSO-treatment showed to slow the proliferation of the cells, which was indicated by the slower doubling time compared to untreated cells (Figure 4.8A).

First TMZ-treatment of T78 cells showed to have a stronger effect on the cell proliferation compared to the second treatment, as the total cell number of the cells for the first treatment is lower compared to the second treatment (Figure 4.6B). After a slight decrease at day 2, the curve showed an ascending tendency at day 3-5. Second TMZ-treatment showed an increasing curve for all five days. Moreover, second TMZ-treatment showed to cross with first DMSO treated cells at day 2 where it also was seen to have a higher cell number at day 3 compared to first DMSO treatment (Figure 4.6B). Doubling times for TMZ-treated cells was found to be faster than both untreated and DMSO-treated cells. Furthermore, the first TMZ-treatment presented a faster doubling time compared to the second treatment. (Figure 4.8B)

First and second TMZ-treatment of T87 cells presented similar proliferation curves and were also similar to both DMSO-treatments (Figure 4.7B). A slight increase in cell number was observed for second TMZ- and DMSO-treatment at day 3 where the number of cells also was seen to increase at day 4 for the TMZ-treated cells. Untreated cells presented the highest number of cells for all five days (Figure 4.7B). Doubling times for both TMZ-treatments showed a minor difference compared to the corresponding DMSO-treatments, where the TMZ treated cells had a faster doubling time. Furthermore, second TMZ treated cells presented a faster doubling time than the cells receiving the first treatment. (Figure 4.8C).

Additionally, an ANOVA test was performed for proliferation curves in order to compare the TMZ-treatments for all three GBM cell line. A statistically significant difference was obtained for the three GBM cell lines ($p= 0.000353$).

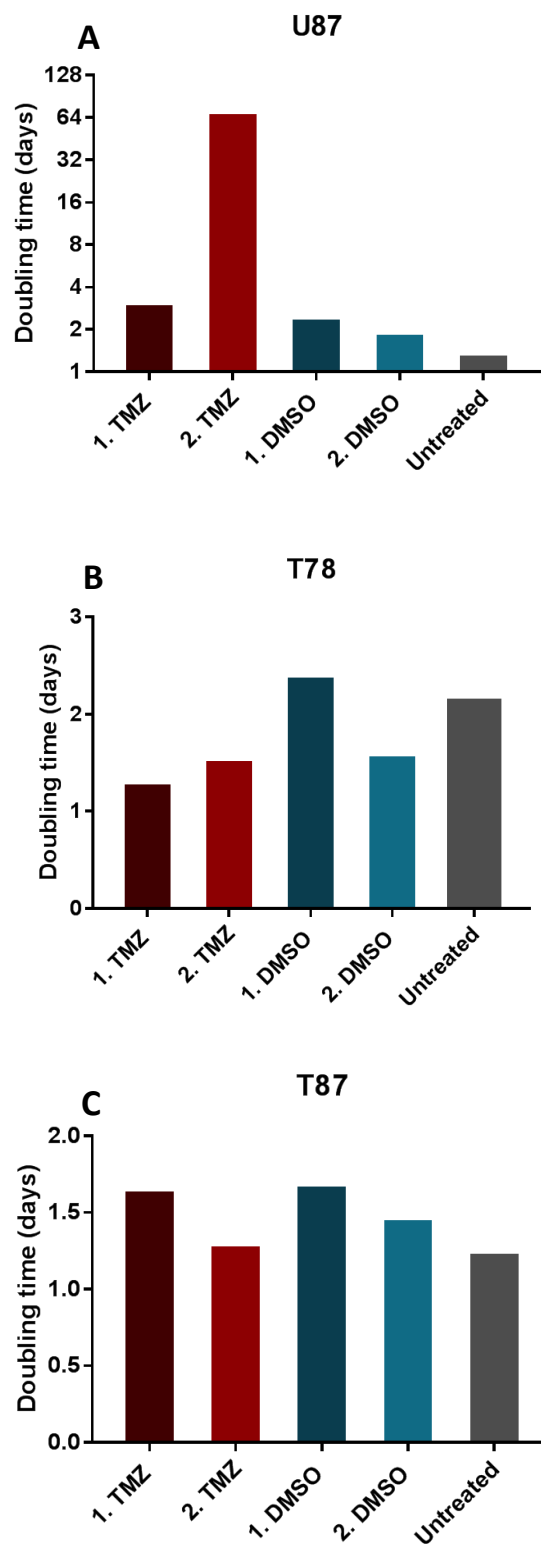


Figure 4.8 Doubling times for GBM cell lines upon double-cycle treatment with TMZ and DMSO
A) Doubling times for U87 **B)** Doubling times for T78 **C)** Doubling times for T87

4.3 – COLONY-FORMING ABILITY OF GBM CELL LINES

To determine the self-renewal ability of GICs after TMZ and DMSO double-cycle treatment, colony-forming unit (CFU) was performed after each rest period. Interestingly, the U87 cells receiving first DMSO-treatment had the highest yield of CFUs and the lowest yield was observed for the cells exposed to second TMZ-treatment (Figure 4.9). Both second TMZ- and DMSO-treatment showed a lower yield compared to the first treatments. The cell lines T78 and T87 only revealed CFU's for one treatment group; T78 cells receiving first DMSO-treatment showed 66.57% whereas T87 cells receiving second TMZ-treatment showed 37.12%.

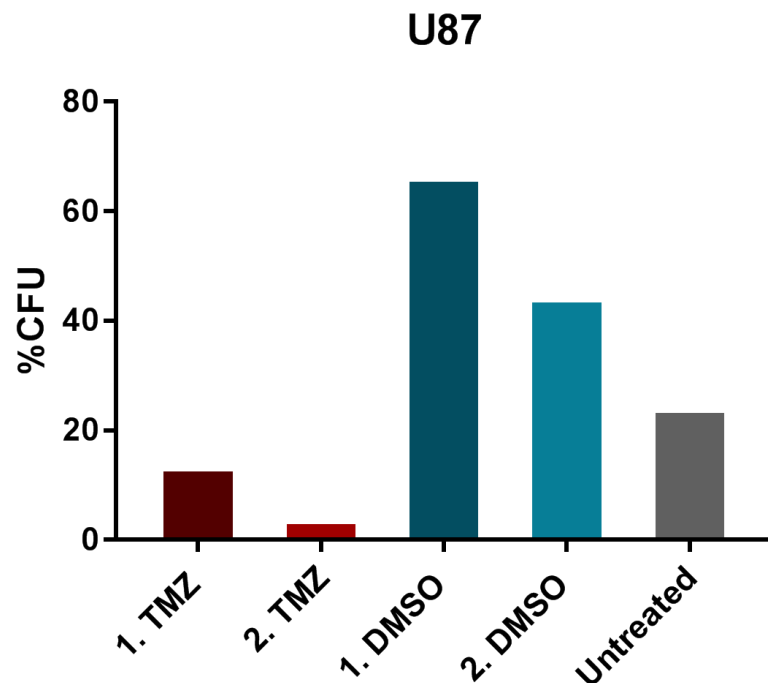


Figure 4.9 Yield of colony-forming unit (CFU) of U87 cells exposed to TMZ double-cycle treatment and DMSO as the control.

4.4 – TRANSCRIPTIONAL ACTIVITY OF THE GENES CCND2, GADD45G, AND CRIPTO-1 AFTER TMZ DOUBLE-CYCLE TREATMENT

qPCR was used to investigate the transcriptional activity of CCND2, GADD45G and CR-1 in GBM cells exposed to TMZ double-cycle treatment.

Figure 4.10 represents the fold changes of the different treatments where the untreated cells were used as controls. The only statistical significant transcriptional activity for U87 cells was present for the first and second DMSO-treatment, where a down regulation of CCND2 occurred (Figure 4.10A). As the CT value was unavailable for CR-1 untreated cells and first TMZ-treatment, the first DMSO-treatment was used as control for second DMSO- and TMZ-treatment (Figure 4.10C). However, no statistical significant difference was seen for these cells too.

T78 cells showed three statistical significant differences; first and second DMSO-treatment showed a down regulation of CCND2 gene (Figure 4.10A) and a minor upregulation of CR-1 for cells receiving second TMZ-treatment (Figure 4.10C). The CT values for T87 untreated cells for all three genes were unavailable, which resulted in the use of first DMSO-treatment groups as controls. No CT value was acquired for the gene CCND2 in first DMSO-treatment leading to the use of second treatment group as the control; this resulted in a elevated statistical significant upregulation of the gene CCND2 for cells receiving first TMZ-treatment, displaying a fold change of 9.8 (Figure 4.10A). Furthermore, a statistical significant downregulation was displayed of the gene GADD45G for cells receiving first and second DMSO-treatment (Figure 4.10CB).

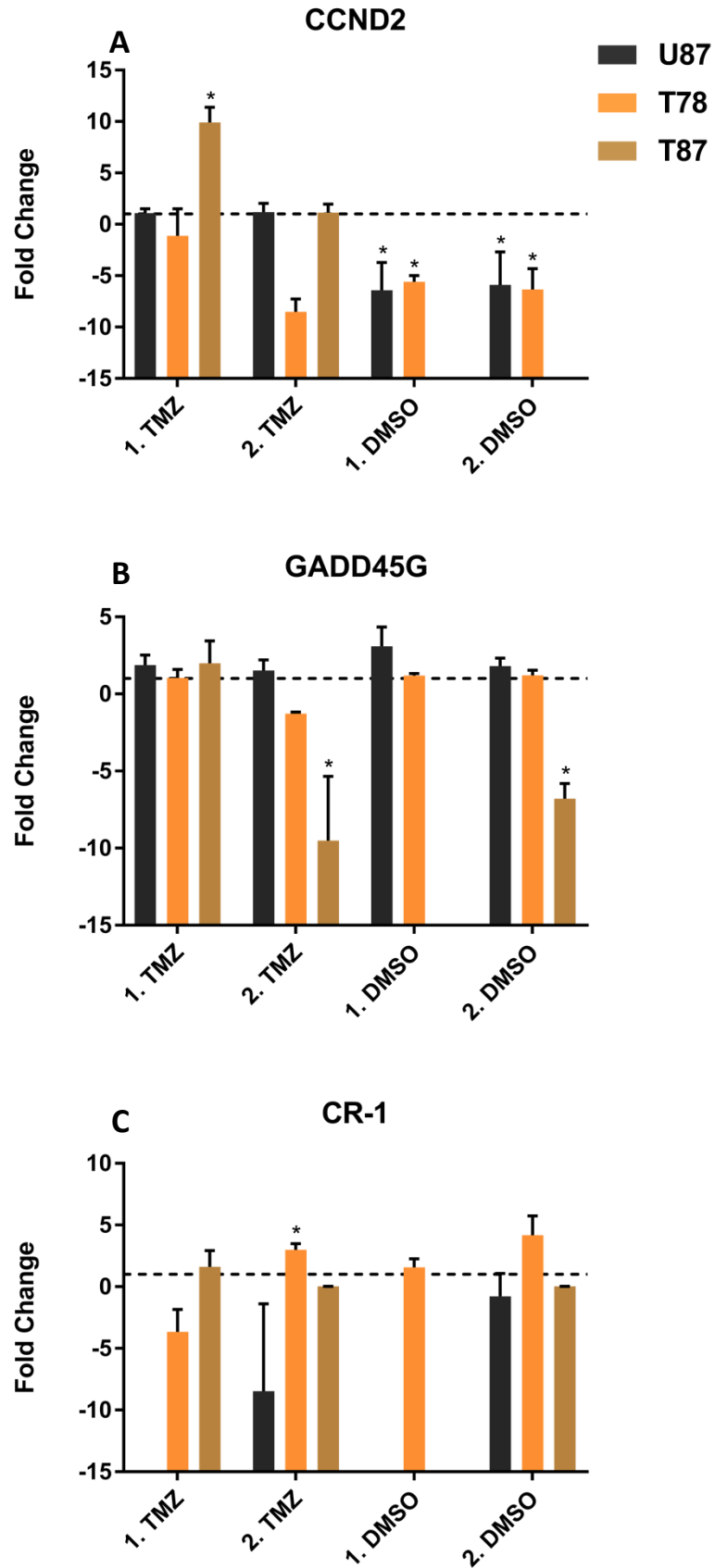


FIGURE 4.10 – Bar charts displaying transcriptional activity of the genes CCND2, GADD45G, and CR-1 for the GBM cell lines U87, T78, and T87 receiving TMZ double-cycle treatment and DMSO-treatment. Untreated samples are used as controls. As no measurements were obtained for T87 untreated samples, the 1. DMSO-treatment was used as the control. Error bars display the standard error of the mean (SEM).

4.5 – CELL PROLIFERATION TRACKING AND CRIPTO-1 EXPRESSION AFTER TMZ-TREATMENT

Flow cytometry was performed in order to track the cell proliferation by CFSE labeling and to investigate the expression of CR-1 after TMZ and DMSO double-cycle treatment.

Figure 4.11 illustrates overlaid graphs for the CFSE-labeled undivided cells and the divided cells three days after CFSE-staining. To analyze the cell proliferation after TMZ- and DMSO treatment, mean fluorescence intensity (MFI) values were acquired using the software FlowJo. MFI values for the cell lines T78 and T87 indicated that the cells did proliferate, when compared to the undivided cell groups (Table 4.1). U87 showed the slowest proliferation among the cell lines. Furthermore, U87 TMZ-treated cells presented a somewhat higher MFI for the undivided cells compared the undivided DMSO group.

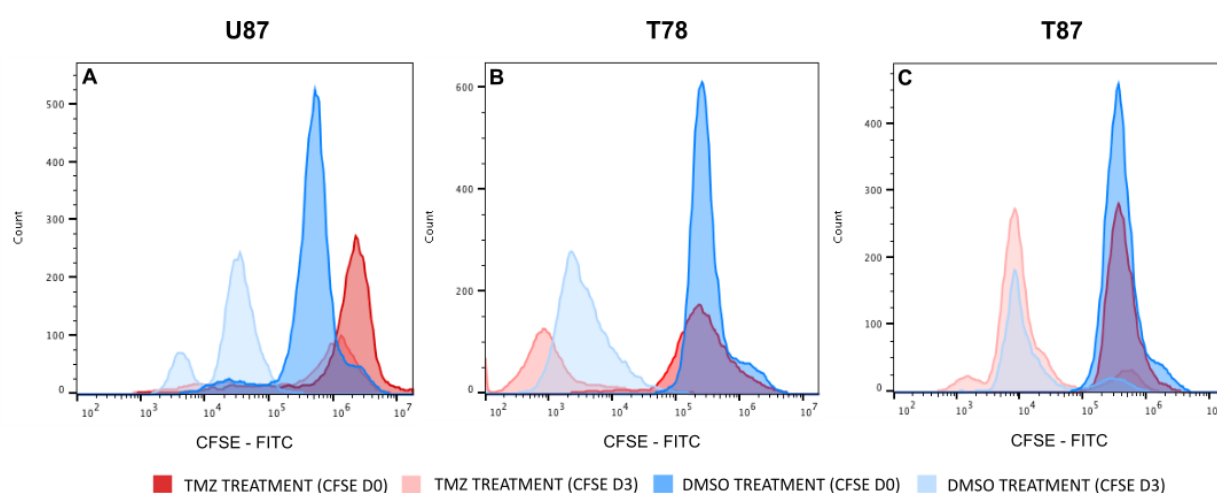


Figure 4.11 Histograms presenting the proliferation activity through fluorescence intensity of CFSE-labeled cells, which received TMZ double-cycle treatment and DMSO treatment as the control group. The dark red and blue coloured histograms represent the undivided cells for TMZ- and DMSO-treated cells, respectively, designated CFSE D0. The lighter red and blue colours represent the CFSE-labeled TMZ- and DMSO-treated cells, harvested after three days of incubation.

Table 4.1 MFI values for undivided CFSE-labelled cells (CFSE D0) and CFSE-labelled cells incubated for three days (CFSE D3).

	U87	T78	T87
DMSO – CFSE D0	375091	276.362	370.710
DMSO – CFSE D3	30.625	3172	10.210
TMZ – CFSE D0	1.250.000	247176	395.455
TMZ – CFSE D3	720.000	6533	9078

To validate the CR-1 antibody used in this study, the staining was performed on the cell lines U87+CR-1 (CR-1 transfected cell line), NTERA-2, and T10, which are known to express CR-1 (Figure 4.12).

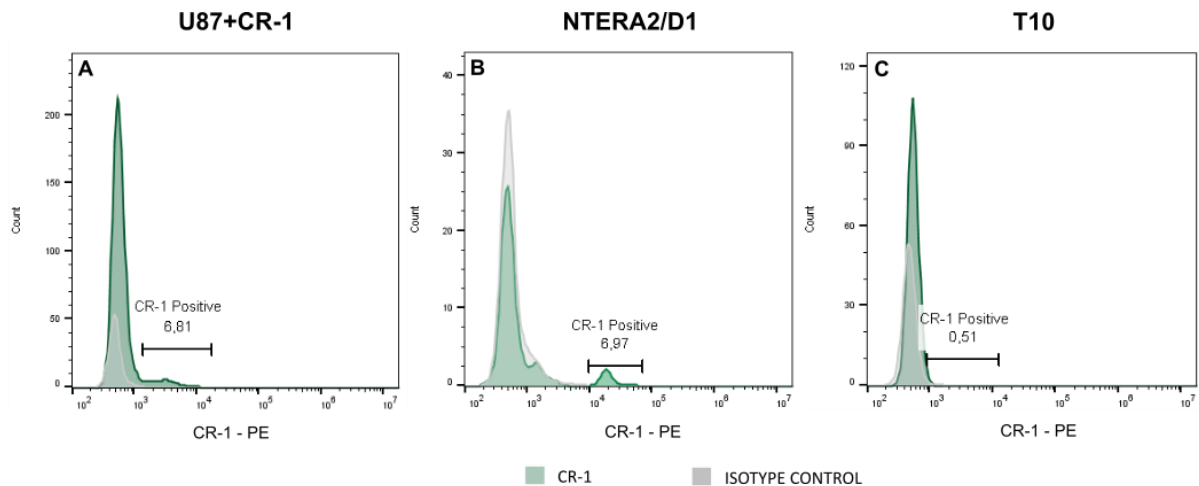


Figure 4.12 Validation of CR-1 antibody by staining three cell lines known to express CR-1

Cr-1 antibody staining of U87 and T87 showed increased fluorescence intensity compared to unspecific isotype staining. However, as the only one, T78 cells treated with TMZ displayed a lower fluorescence intensity compared to the isotype control (Figure 4.13; Table 4.1). U87 and T78 cells treated with TMZ presented a lower percentage of CR-1 positive cells compared DMSO treated cells whereas T87 TMZ treated cells showed a higher percentage of CR-1 positive cells than the DMSO group (Table 4.2).

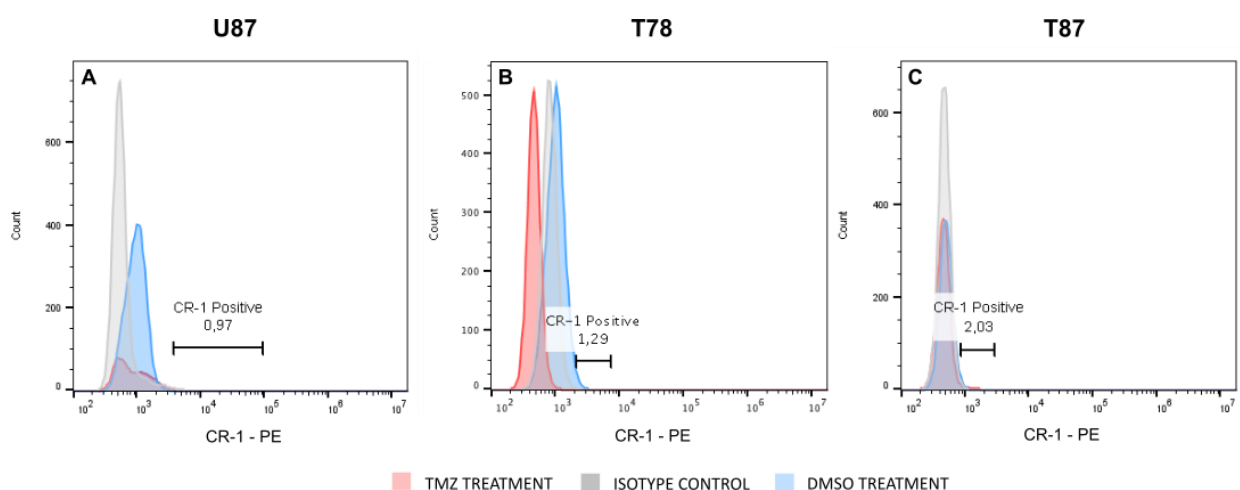


FIGURE 4.13 Analysis of CR-1 expression of U87, T78, and T87 receiving TMZ and DMSO double-cycle treatment. The cell harvesting was performed in the end of the second TMZ- and DMSO-treatments.

TABLE 4.2 – Percentage of CR-1 positive cells after double-cycle treatments

	TMZ TREATMENT	DMSO TREATMENT
U87	0,64%	1,19%
T78	1,15%	1,29%
T87	2,42%	1,98%

5 – DISCUSSION

In this study, three GBM cell lines were exposed to the cytostatic TMZ, where the treatment comprised a double cycle including periods with and without treatment. DMSO-treated cells were used as the vehicle control group. The cells were analyzed after both first and second treatment cycles in regards to the effect of TMZ on cell viability and proliferation, self-renewal ability, DNA-damage repair mechanism, and CR-1 expression. Results obtained from the present study are discussed below.

The three GBM cell lines U87, T78, and T87 responded differently to TMZ double-cycle treatment, which was confirmed by statistical analysis. U87 demonstrated to be the most TMZ sensitive cell line compared to the two primary cell lines. Cell viability was decreased upon both TMZ-treatments, where the lowest viability was detected after second treatment. Inhibition of cancer cell proliferation is known to be crucial for ascertaining the success of the treatment. Assays regarding U87 cell proliferation revealed that the cells were severely affected by the second TMZ-treatment as almost no cell proliferation occurred. As the only cell line, TMZ double-cycle treatment has also shown to affect the self-renewal ability of U87 cells, which may indicate an effect of TMZ on GICs as well. However, the DMSO-treated cells showed a higher clonogenicity compared to the TMZ-treated group. The expectation was that GICs would survive therapeutic selection pressure by TMZ so the CFU assays showing increased clonogenicity of DMSO-treated cells and decreased clonogenicity for TMZ-treated cells are inexplicable results.

The effect of TMZ on CR-1 expression levels was investigated in order to explore its relation to the self-renewal capacity of GICs. Although no statistically significant differences were obtained from the transcriptional activity of the gene, TMZ double-cycle treatment showed to reduce the CR-1 expression for the cell line U87. Inhibition of the self-renewal ability and proliferation of U87 cells upon TMZ treatment could suggest a correlation between the known self-renewal ability of GICs and CR-1 expression levels. Assumed that CR-1 is a marker for GICs, the findings for the cell line U87 contradicts with the theory of GICs being resistance to chemotherapy. Similar results were obtained for a study by Beier *et al*,

which treated primary GBM cells, consisting of CD133-positive cells suggested to comprise GICs, with TMZ with increasing doses of 5, 50, and 500 $\mu\text{mol/L}$. The results indicated that TMZ-treatments reduce the clonogenicity of GICs, which again do not contribute to the chemoresistance theory (51). However, it must be taken into account that other studies have shown that CD133-negative population also displayed similar tumor-forming properties and therefore the validity of CD133 as a marker for GICs still remains controversial (30,31).

A possible explanation for how U87 cells responded to the TMZ double-cycle treatment could be due to the fact that the cell line no longer have the abilities of GICs and that it has lost the genetic traits from the initial tumor. U87 xenograft models have demonstrated that tumors derived from the cell line have a tennis ball appearance without infiltration into the normal brain tissue (52,53). Infiltration is a key feature of GBM invasiveness and thereby the use of this model might give a deceitful efficacy of TMZ for GBM patients.

Different findings were obtained for the primary cell lines. T78 and T87 were reported to have a methylated MGMT promoter, indicating that a possible TMZ sensitivity of both cell lines were independent from MGMT interaction. For T78, TMZ cytotoxicity was seen to strongly affect the cell viability upon first TMZ-treatment where a revival was observed after the second treatment; this corresponded with results obtained for cell proliferation. Interestingly, the results revealed that the TMZ-treated cells had faster proliferation compared to both the untreated cells and the DMSO control group. Previously mentioned study by Beier *et al* demonstrated that upon TMZ-treatment, CD133⁺ cells proliferated faster than CD133⁻ cells. This gave rise to the questioning about whether the inevitable growth of GBM could be due to rapid proliferation of GICs (51).

Additionally, T78 showed a significant upregulation of CR-1 upon second TMZ-treatment with a fold change of 2.94. Morphological and proliferation analysis of the cell line revealed a revival process during second treatment cycle, which might suggest a connection between the cell revival and CR-1 expression. Findings for the functional features of T78 and elevated CR-1 levels could indicate a developed TMZ resistance after first TMZ cycle-treatment. A previous study has shown an elevation upon TMZ-treatment of the GIC marker Sox2, which revealed to contribute to regulation of stem cell properties and chemoresistance (54). In the present study, the melt curve analysis of the CR-1 gene should be taken into account, as several peaks were observed, suggesting that the detected amplicon may not be the desired CR-1 (appendix 2). Moreover, CR-1 flow cytometric analysis revealed that TMZ-treated T78 cells were more negative than the isotype control, as it was an unstained sample. The experimental setup was repeated twice in order to eliminate a methodological source of error, however, the same result was obtained both

times. Unfortunately, it has not been possible to find an answer for why the cells responded differently to CR-1 antibody staining in the literature.

T78 cell line has been identified as a mesenchymal GBM subtype, which is known to display a shorter overall survival time. The findings obtained in this study supports the association of mesenchymal subtype being one of the aggressive GBM subtypes. However, a study by Verhaak *et al*, showed that the mesenchymal group significantly reduced mortality upon aggressive treatment comprising chemo- and radiationtherapy, which is inconsistent with the known aggressiveness of the subtype (7). In the present study, the T78 cells showed resistance to TMZ upon second treatment cycle and therefore additional TMZ treatment-cycles might be needed to observe how T78 cells respond to further treatment. The difference in behavior upon first and second TMZ treatment cycle could be due to the link between the mesenchymal group and EMT process, which is associated with higher degree of tumor invasiveness. Further investigations are, however, required to investigate this linkage.

The effect of TMZ-treatment on T87 showed to be different than the other two cell lines. The cell line demonstrated the same features as the DMSO control group regarding morphology, cell proliferation, and doubling time. However, inhibition of the colony-formation was shown after second TMZ-treatment, which did not correlate with the other findings. The overall findings may be associated with which GBM subtype the cell line belongs to. A former characterization of T87 performed by Jensen *et al*. identified the cell line as a proneural subtype. The same study identified the proneural T87 as the most invasive compared to the cell lines T78 and T87, which belong to the mesenchymal and classical subtype, respectively. The results in the present study contradict with the assumption that the proneural subtype has a better prognosis compared to the other subtype, as the cell line did not respond to the treatment.

No statistically significant results were obtained for the transcriptional activity of CR-1, however, as the only cell line, the percentage of CR-1 positive cells were increased upon TMZ treatment. The increased CR-1 expression and the decreased self-renewal ability observed for T87 upon second TMZ treatment contradicts with the probable correlation of CR-1 and GICs. The reliability of the CFU assays may have an influence on this result, as the assays only have been performed once.

Remarkably, the control DMSO-treatment also showed to exert an effect on all three cell lines when compared to untreated cells. A statistical significant downregulation of the proliferation gene CCND2 for U87, T78, and T87 upon both first and second DMSO-treatment were showed, which correlated with the findings obtained from proliferation curves. DMSO is widely used as a solvent for TMZ, which is not soluble in water, and as vehicle

control groups. However, there are different opinions concerning concentration due to toxicity. Final concentration ranging from 0.5-1.5% is reported to be used for cell culture and in vivo experiments (55). Other studies have demonstrated that different cell types have different DMSO thresholds, which may affect the cell viability and growth. Chinese hamster ovary (CHO) cells have for example demonstrated a threshold dose of 0.5%, where it was reported to be 1% for choriocapillary endothelial cells. (56–58)

In the present study, 0.4% DMSO was applied and inhibition of cellular proliferation was detected for all GBM cell lines. This gives rise to questioning about whether it is the solvent DMSO that exerts the effect on the cells or TMZ. For the cell line T87, it was clear that the variation of TMZ-treated cells from the untreated cells was due to DMSO. Interestingly for T87 cells, the gene GADD45G, which was used as an indicator for DNA damage, was significantly downregulated upon second TMZ- and DMSO-treatment compared to the first DMSO-treatment. Transcriptional levels of GADD45G are known to increase following treatment with DNA-damaging agents as the gene is known to be involved in inhibition of cell proliferation and increased apoptosis in response to drug treatment (50,59). A down-regulation will lead to increased cell proliferation, which also corresponded with the results for proliferation curves for the cell line.

6 – CONCLUSION

The present study investigated the effect of selection pressure with the cytostatic TMZ on functional features in GBM in vitro models. Furthermore, the effect of TMZ treatment on CR-1 expression and its relation to the self-renewal ability of GICs was explored. A TMZ double-cycle treatment was applied in order to mimic the treatment cycles patients receive in the clinic.

A statistical significant difference in response to TMZ-treatments was obtained for all three GBM cell lines. The model GBM cell line U87 demonstrated to be TMZ-sensitive upon double-cycle treatment. Decrease in cell viability, proliferation, and self-renewal ability as well as CR-1 expression were observed suggesting that GICs may be TMZ-sensitive, which contradicts with the hypothesis of GICs ability to escape chemotherapy. Otherwise, the cell line could have lost the abilities of GICs and therefore respond severely to TMZ-treatment. MGMT-methylated primary cell line T78 did not respond to TMZ-treatment upon second treatment and a significant upregulation was detected for CR-1 transcriptional activity; this suggested a correlation between the possible GIC marker CR-1 and chemoresistance. T87 did not respond to both first and second TMZ treatment cycle regarding functional features. However, CR-1 positive cells were shown to increase upon second TMZ-treatment for T87. Furthermore, the control DMSO-treatment showed to exert a cytotoxic effect on all cell lines resulting in doubts about the actual effect of TMZ.

Overall, the three GBM cell lines responded differently to the TMZ double-cycle treatment, which may be related to their genetic tumor profiles. The results obtained in this study were inconclusive in order to detect GICs ability of escaping chemotherapy by the use of CR-1 as a marker for the population. Further studies are therefore required in order to investigate the effect of TMZ on GBM in vitro models and how the GIC population is affected by the TMZ-treatment.

7 – FUTURE APPLICATIONS

In the present study, the results obtained for primary cell lines T78 and T87 showed therapy resistance to TMZ in a concentration of 50 $\mu\text{mol/L}$. Other studies have used this concentration as one of the lowest concentrations, which could suggest that an experimental set-up with higher doses of TMZ could be performed. It would be interesting to investigate how the cells would react to stronger treatment to see if they still preserve their resistance to TMZ. Additionally, it could be relevant to include further cycle treatments, especially for the mesenchymal T78, which showed to react differently upon first and second TMZ-treatment. Further functional assays as for example migration assay could also be included to investigate the migratory abilities of the cell lines following TMZ-treatment.

It could be speculated that the effect of TMZ on GIC population could be investigated through a combination of different GIC markers both to compare how CR-1 expression is affected compared to the other markers and to obtain a better understanding of GBM subtype variation. As the mesenchymal subtype is linked to the EMT process, investigating different EMT markers would provide a better understanding to why T78 cells react differently upon first and second TMZ-treatment.

BIBLIOGRAPHY

1. Wilson T, Karajannis M, Harter D. Glioblastoma multiforme: State of the art and future therapeutics. *Surg Neurol Int* [Internet]. 2014;5(1):64. Available from: <http://surgicalneurologyint.com/surgicalint-articles/glioblastoma-multiforme-state-of-the-art-and-future-therapeutics/>
2. Hanif F, Muzaffar K, Perveen K, Malhi SM, Simjee SU. Glioblastoma Multiforme: A Review of its Epidemiology and Pathogenesis through Clinical Presentation and Treatment. *Asian Pac J Cancer Prev* [Internet]. 2017;18(1):3–9. Available from: <http://www.ncbi.nlm.nih.gov/pubmed/28239999>
<http://www.pubmedcentral.nih.gov/articlerender.fcgi?artid=PMC5563115>
3. Alifieris C, Trafalis DT. Glioblastoma multiforme: Pathogenesis and treatment. *Pharmacol Ther*. 2015;152:63–82.
4. Carlsson SK, Brothers SP, Wahlestedt C. Emerging treatment strategies for glioblastoma multiforme. *EMBO Mol Med* [Internet]. 2014;6(11):1359–70. Available from: <http://embomolmed.embopress.org/cgi/doi/10.15252/emmm.201302627>
5. Louis DN, Ohgaki H, Wiestler OD, Cavenee WK, Burger PC, Jouvet A, et al. The 2007 WHO classification of tumours of the central nervous system. *Acta Neuropathol*. 2007;114(2):97–109.
6. Davis ME. Glioblastoma: Overview of Disease and Treatment. *Clin J Oncol Nurs*. 2016;20(5):1–14.
7. Verhaak RGW, Hoadley KA, Purdom E, Wang V, Qi Y, Wilkerson MD, et al. An integrated genomic analysis identifies clinically relevant subtypes of glioblastoma characterized by abnormalities in PDGFRA, IDH1, EGFR and NF1. *Cancer Cell* [Internet]. 2010;19(1):1–25. Available from: <http://www.pubmedcentral.nih.gov/articlerender.fcgi?artid=2886992&tool=pmcentrez&rendertype=abstract>
8. Lin N, Yan W, Gao K, Wang Y, Zhang J, You Y. Prevalence and clinicopathologic characteristics of the molecular subtypes in malignant glioma: A multi-institutional analysis of 941 cases. *PLoS One*. 2014;9(4):1–5.
9. Phillips HS, Kharbanda S, Chen R, Forrest WF, Soriano RH, Wu TD, et al. Molecular subclasses of high-grade glioma predict prognosis, delineate a pattern of disease progression, and resemble stages in neurogenesis. *Cancer Cell*. 2006;9(3):157–73.
10. Elias MC, Tozer KR, Silber JR, Mikheeva S, Deng M, Morrison RS, et al. TWIST is expressed in human gliomas and promotes invasion. *Neoplasia* [Internet]. 2005;7(9):824–37. Available from: <http://www.ncbi.nlm.nih.gov/pubmed/16229805>
<http://www.pubmedcentral.nih.gov/articlerender.fcgi?artid=PMC1501937>
11. Tso C-L, Shintaku P, Chen J, Liu Q, Liu J, Chen Z, et al. Primary Glioblastomas Express Mesenchymal Stem-Like Properties. *Mol Cancer Res* [Internet]. 2006;4(9):607–19. Available from: <http://mcr.aacrjournals.org/cgi/doi/10.1158/1541-7786.MCR-06-0005>
12. Jackson M, Hassiotou F, Nowak A. Glioblastoma stem-like cells: At the root of tumor recurrence and a therapeutic target. *Carcinogenesis*. 2014;36(2):177–85.
13. Minniti G, Muni R, Lanzetta G, Marchetti P, Maurizi Enrici R. Chemotherapy for glioblastoma: Current

treatment and future perspectives for cytotoxic and targeted agents. *Anticancer Res.* 2009;29(12):5171–84.

14. Mallick S, Benson R, Hakim A, Rath GK. Management of glioblastoma after recurrence: A changing paradigm. *J Egypt Natl Canc Inst [Internet].* National Cancer Institute, Cairo University; 2016;28(4):199–210. Available from: <http://dx.doi.org/10.1016/j.jnci.2016.07.001>
15. Yong RL, Lonser RR. Surgery for glioblastoma multiforme: striking a balance. 2011;1–5.
16. Zhang J, F.G. Stevens M, D. Bradshaw T. Temozolomide: Mechanisms of Action, Repair and Resistance. *Curr Mol Pharmacol [Internet].* 2012;5(1):102–14. Available from: <http://www.eurekaselect.com/openurl/content.php?genre=article&issn=1874-4672&volume=5&issue=1&spage=102>
17. Lee SY. Temozolomide resistance in glioblastoma multiforme. *Genes Dis. Elsevier Ltd;* 2016;3(3):198–210.
18. Barciszewska AM, Gurda D, Głodowicz P, Nowak S, Naskręt-Barciszewska MZ. A new epigenetic mechanism of temozolomide action in glioma cells. *PLoS One.* 2015;10(8).
19. Stupp R, Mason W, Bent M van den, Weller M, Fisher B, Taphoorn M, et al. Radiotherapy plus concomitant and adjuvant temozolomide for glioblastoma. *N Engl J Med.* 2005;352:987–96.
20. Side effects of temozolomide (Temodal) [Internet]. Cancer Research UK. [cited 2018 May 26]. Available from: <http://www.cancerresearchuk.org/about-cancer/cancer-in-general/treatment/cancer-drugs/drugs/temozolomide/side-effects>
21. Thon N, Kreth S, Kreth F-W. Personalized treatment strategies in glioblastoma: MGMT promoter methylation status. *Onco Targets Ther [Internet].* 2013;6:1363–72. Available from: <http://www.ncbi.nlm.nih.gov/pubmed/24109190%5Cnhttp://www.pubmedcentral.nih.gov/articlerender.fcgi?artid=PMC3792931>
22. Dresemann G. Temozolomide in malignant glioma. *Onco Targets Ther.* 2010;3:139–46.
23. Cheng L, Wu Q, Guryanova OA, Huang Z, Huang Q, Rich JN, et al. Elevated invasive potential of glioblastoma stem cells. *Biochem Biophys Res Commun [Internet].* Elsevier Inc.; 2011;406(4):643–8. Available from: <http://dx.doi.org/10.1016/j.bbrc.2011.02.123>
24. Bianco C, Rangel MC, Castro NP, Nagaoka T, Rollman K, Gonzales M, et al. Role of Cripto-1 in stem cell maintenance and malignant progression. *Am J Pathol.* 2010;177(2):532–40.
25. Agnihotri S, Munoz D, Zadeh G, Guha A. Brain tumor-initiating cells and cells of origin in glioblastoma. *Transl Neurosci.* 2011;2(4):331–8.
26. Ahmed AU, Auffinger B, Lesniak MS. Understanding glioma stem cells: rationale, clinical relevance and therapeutic strategies. *Expert Rev Neurother.* 2015;13(5):545–55.
27. Auffinger B, Spencer D, Pytel P, Ahmed AU, Lesniak MS. The role of glioma stem cells in chemotherapy resistance and glioblastoma multiforme recurrence. *Expert Rev Neurother.* 2016;15(7):741–52.
28. Liebelt BD, Shingu T, Zhou X, Ren J, Shin SA, Hu J. Glioma Stem Cells: Signaling, Microenvironment, and Therapy. *Stem Cells Int.* 2016;2016.

29. Singh SK, Climate B, Dyck V, Phylogenies TF, Compare EP, Hawkins C, et al. Identification of human brain tumour initiating cells. *Nature* [Internet]. 2004;432(November):396–401. Available from: <http://dx.doi.org/10.1038/nature03128>
30. Clément V, Dutoit V, Marino D, Dietrich PY, Radovanovic I. Limits of CD133 as a marker of glioma self-renewing cells. *Int J Cancer*. 2009;125(1):244–8.
31. Sergey V. Shmelkov, Jason M. Butler, Andrea T. Hooper, Adilia Hormigo, Jared Kushner, Till Milde, Ryan St. Clair, Muhamed Baljevic, Ian White, David K. Jin, Amy Chadburn, Andrew J. Murphy, David M. Valenzuela, Nicholas W. Gale, Gavin Thurston, George D. Y SR. CD133 expression is not restricted to metastatic colon cancer cells initiate tumors. *J Clin Invest* [Internet]. 2008;118(6):2111–20. Available from: www.jci.org/articles/view/34401
32. Watanabe K, Meyer MJ, Strizzi L, Lee JM, Bianco C, Nagaoka T, et al. Cripto-1 Is a Cell Surface Marker for a Tumorigenic, Undifferentiated Subpopulation in Human Embryonal Carcinoma Cells. 2010;28(8):1303–14.
33. Klauzinska M, Castro NP, Rangel MC, Spike BT, Gray PC, Bertolette D, et al. The multifaceted role of the embryonic gene Cripto-1 in cancer, stem cells and epithelial-mesenchymal transition. *Semin Cancer Biol* [Internet]. Elsevier Ltd; 2014;29(C):51–8. Available from: <http://dx.doi.org/10.1016/j.semcancer.2014.08.003>
34. Ebert AD, Wechselberger C, Nees M, Clair T, Schaller G, Martinez-Lacaci I, et al. Cripto-1-induced increase in vimentin expression is associated with enhanced migration of human Caski cervical carcinoma cells. *Exp Cell Res*. 2000;257(1):223–9.
35. Bianco C, Salomon DS. Targeting the embryonic gene Cripto-1 in cancer and beyond. 2010;20(12):1739–49.
36. Pauklin S, Vallier L. Activin/Nodal signalling in stem cells. *Development* [Internet]. 2015;142(4):607–19. Available from: <http://dev.biologists.org/cgi/doi/10.1242/dev.091769>
37. Strizzi L, Bianco C, Normanno N, Salomon D. Cripto-1: A multifunctional modulator during embryogenesis and oncogenesis. *Oncogene*. 2005;24(37):5731–41.
38. Mahmoudian RA, Abbaszadegan MR, Forghanifard MM, Moghbeli M, Moghbeli F, Chamani J, et al. Biological and Clinicopathological Significance of Cripto-1 Expression in the Progression of Human ESCC. *Reports Biochem Mol Biol* [Internet]. 2017;5(2):83–90. Available from: <http://www.ncbi.nlm.nih.gov/pubmed/28367468>
39. Strizzi L, Bianco C, Normanno N, Seno M, Wechselberger C, Wallace-Jones B, et al. Epithelial mesenchymal transition is a characteristic of hyperplasias and tumors in mammary gland from MMTV-Cripto-1 transgenic mice. *J Cell Physiol*. 2004;201(2):266–76.
40. Rangel MC, Karasawa H, Castro NP, Nagaoka T, Salomon DS, Bianco C. Role of Cripto-1 during epithelial-to-mesenchymal transition in development and cancer. *Am J Pathol* [Internet]. Elsevier Inc.; 2012;180(6):2188–200. Available from: <http://dx.doi.org/10.1016/j.ajpath.2012.02.031>
41. Larue L, Bellacosa A. Epithelial-mesenchymal transition in development and cancer: Role of phosphatidylinositol 3' kinase/AKT pathways. *Oncogene*. 2005;24(50):7443–54.
42. Zeisberg M, Neilson EG. Biomarkers for epithelial-mesenchymal transitions. 2009;119(6):1429–37.

43. Castro Pereira N, Rangel MC, Nagaoka T, Karasawa H, Salomon DS, Bianco C. Cripto-1: At the Crossroads of Embryonic Stem Cells and Cancer. *Basic Biol to Bioeng* [Internet]. 2011; Available from: <http://dx.doi.org/10.5772/22800%5CnDO>
44. Strizzi L, Postovit L-M, Marganyan N V., Seftor EA, Abbott DE, Seftor RE., et al. Emerging Roles of Nodal and Cripto-1: From Embryogenesis to Breast Cancer Progression. 2008;1–21.
45. Tysnes BB, Sætran HA, Mørk SJ, Margaryan N V., Eide GE, Petersen K, et al. Age-Dependent Association between Protein Expression of the Embryonic Stem Cell Marker Cripto-1 and Survival of Glioblastoma Patients. *Transl Oncol* [Internet]. 2013;6(6):732-IN33. Available from: <http://linkinghub.elsevier.com/retrieve/pii/S1936523313800137>
46. Pilgaard L, Mortensen JH, Henriksen M, Olesen P, Sørensen P, Laursen R, et al. Cripto-1 expression in glioblastoma multiforme. *Brain Pathol*. 2014;24(4):360–70.
47. Jensen SS, Aaberg-Jessen C, Andersen C, Schrøder HD, Kristensen BW. Glioma spheroids obtained via ultrasonic aspiration are viable and express stem cell markers: A new tissue resource for glioma research. *Neurosurgery*. 2013;73(5):868–86.
48. Jensen SS, Meyer M, Petterson SA, Halle B, Rosager AM, Aaberg-Jessen C, et al. Establishment and characterization of a tumor stem cell-based glioblastoma invasion model. *PLoS One* [Internet]. 2016;11(7). Available from: <http://dx.doi.org/10.1371/journal.pone.0159746>
49. Smith D, Mann D, Yong K. Cyclin D type does not influence cell cycle response to DNA damage caused by ionizing radiation in multiple myeloma tumours. *Br J Haematol*. 2016;173(5):693–704.
50. Tamura RE, Vasconcellos JF de, Sarkar D, Libermann TA, Fisher PB, Zerbini LF. GADD45 proteins: central players in tumorigenesis. 2012;1–31.
51. Beier D, Röhl S, Pillai DR, Schwarz S, Kunz-Schughart LA, Leukel P, et al. Temozolomide preferentially depletes cancer stem cells in glioblastoma. *Cancer Res*. 2008;68(14):5706–15.
52. Radaelli E, Ceruti R, Patton V, Russo M, Degrassi A, Croci V, et al. Immunohistopathological and neuroimaging characterization of murine orthotopic xenograft models of glioblastoma multiforme recapitulating the most salient features of human disease. 2009;879–91.
53. de Vries NA, Beijnen JH, van Tellingen O. High-grade glioma mouse models and their applicability for preclinical testing. *Cancer Treat Rev* [Internet]. Elsevier Ltd; 2009;35(8):714–23. Available from: <http://dx.doi.org/10.1016/j.ctrv.2009.08.011>
54. Garros-Regulez L, Aldaz P, Arrizabalaga O, Moncho-Amor V, Carrasco-Garcia E, Manterola L, et al. mTOR inhibition decreases SOX2-SOX9 mediated glioma stem cell activity and temozolomide resistance. *Expert Opin Ther Targets* [Internet]. Taylor & Francis; 2016;20(4):393–405. Available from: <http://www.tandfonline.com/doi/full/10.1517/14728222.2016.1151002>
55. Yuan C, Gao J, Guo J, Bai L, Marshall C, Cai Z, et al. Dimethyl sulfoxide damages mitochondrial integrity and membrane potential in cultured astrocytes. *PLoS One*. 2014;9(9).
56. Zhang C, Deng Y, Dai H, Zhou W, Tian J, Bing G, et al. Effects of dimethyl sulfoxide on the morphology and viability of primary cultured neurons and astrocytes. *Brain Res Bull* [Internet]. Elsevier Inc.; 2017;128:34–9. Available from: <http://dx.doi.org/10.1016/j.brainresbull.2016.11.004>
57. Liu C-H, Chen L-H. Promotion of recombinant macrophage colony stimulating factor production by

dimethyl sulfoxide addition in Chinese hamster ovary cells. *J Biosci Bioeng* [Internet]. 2007;103(1):45–9. Available from: <http://linkinghub.elsevier.com/retrieve/pii/S1389172307700233>

58. Eter N, Spitznas M. DMSO mimics inhibitory effect of thalidomide on choriocapillary endothelial cell proliferation in culture. *Br J Ophthalmol*. 2002;86(11):1303–5.
59. NCBI. GADD45G growth arrest and DNA damage inducible gamma [*Homo sapiens* (human)] [Internet]. [cited 2018 May 28]. Available from: <https://www.ncbi.nlm.nih.gov/gene/10912>

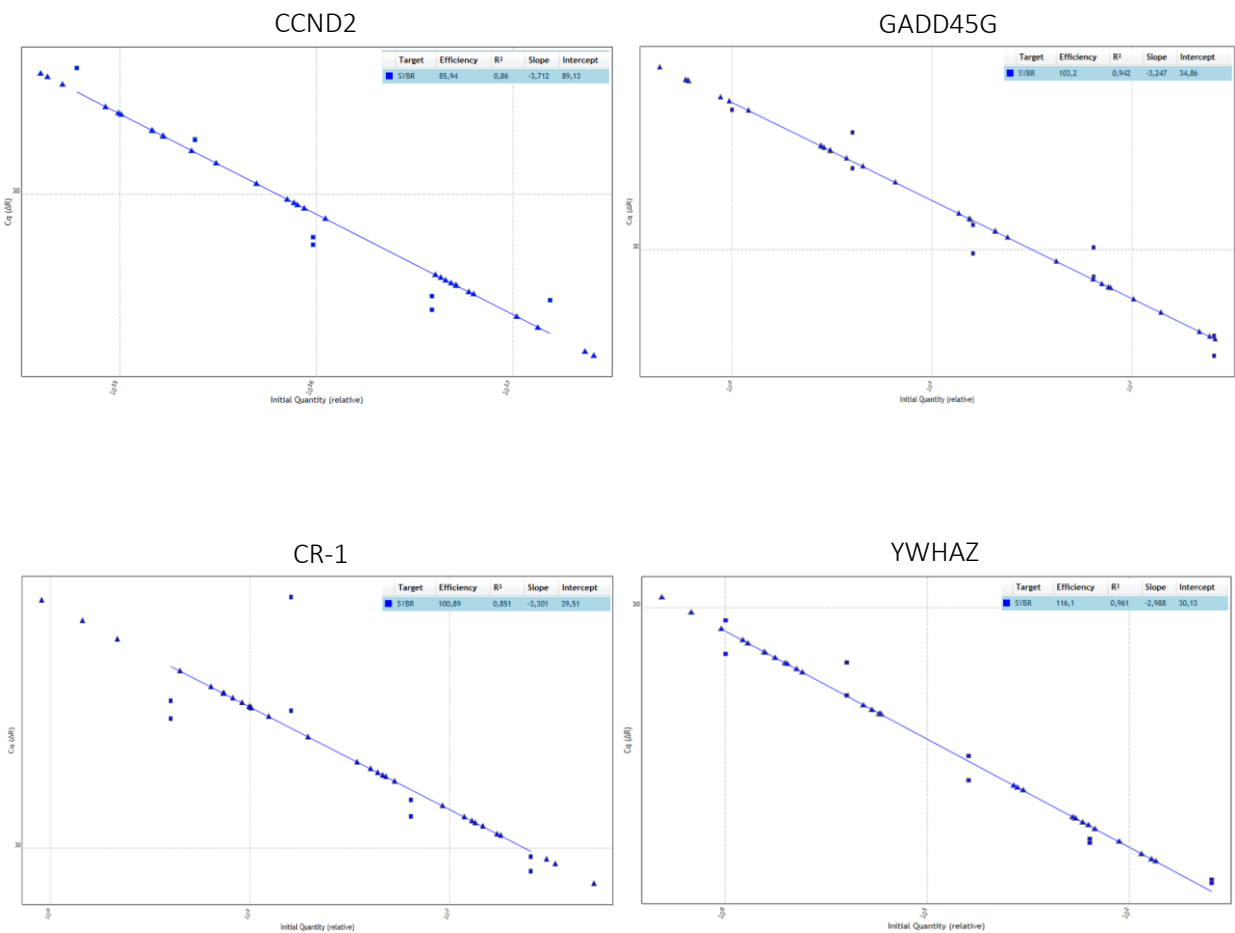
APPENDIX

APPENDIX 1 – COLONY-FORMING UNIT (CFU) ASSAY PLATE SETUP

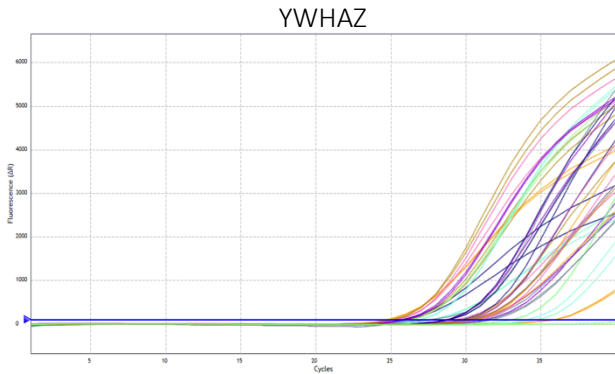
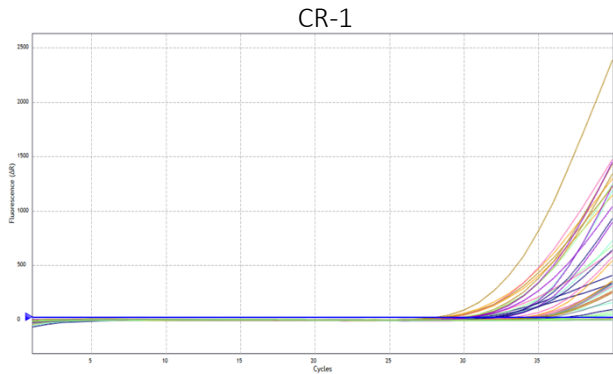
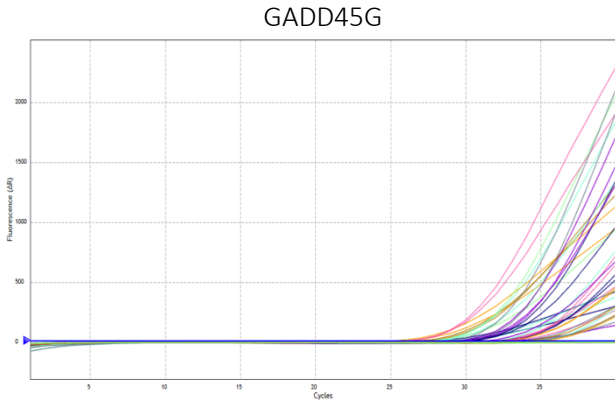
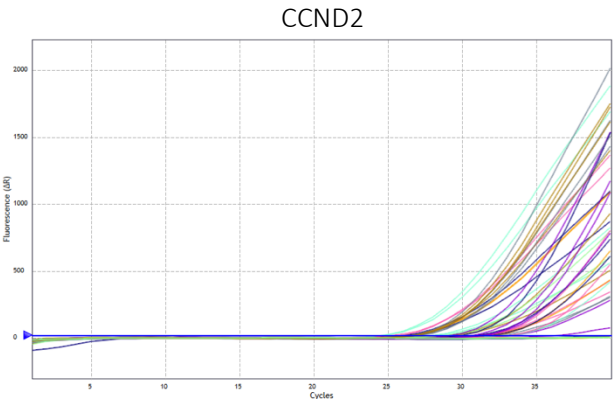
	1	2	3	4	5	6	7	8	9	10	11	12
A	100	100	50	50	25	25	12.5	12.5	6,25	6,25	3.125	3.125
B	100	100	50	50	25	25	12.5	12.5	6,25	6,25	3.125	3.125
C	100	100	50	50	25	25	12.5	12.5	6,25	6,25	3.125	3.125
D	100	100	50	50	25	25	12.5	12.5	6,25	6,25	3.125	3.125
E	100	100	50	50	25	25	12.5	12.5	6,25	6,25	3.125	3.125
F	100	100	50	50	25	25	12.5	12.5	6,25	6,25	3.125	3.125
G	100	100	50	50	25	25	12.5	12.5	6,25	6,25	3.125	3.125
H	100	100	50	50	25	25	12.5	12.5	6,25	6,25	3.125	3.125

APPENDIX 2 – QPCR DATA OUTPUT

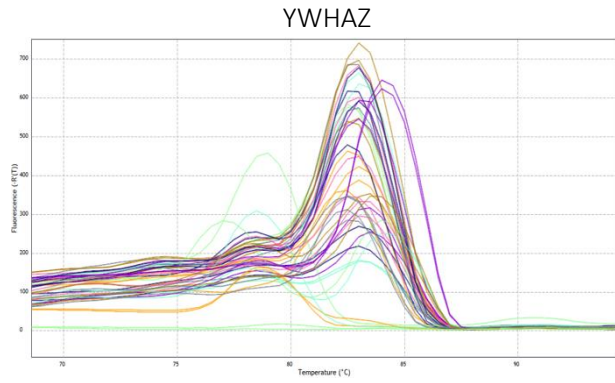
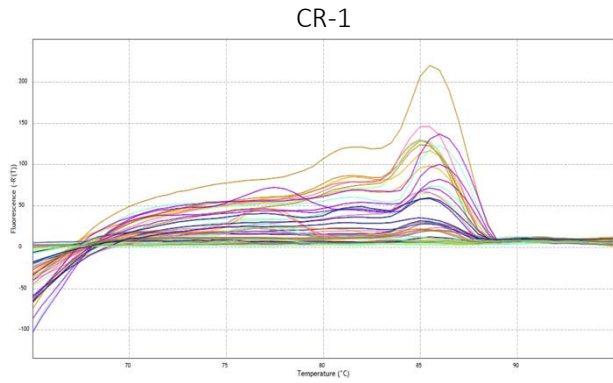
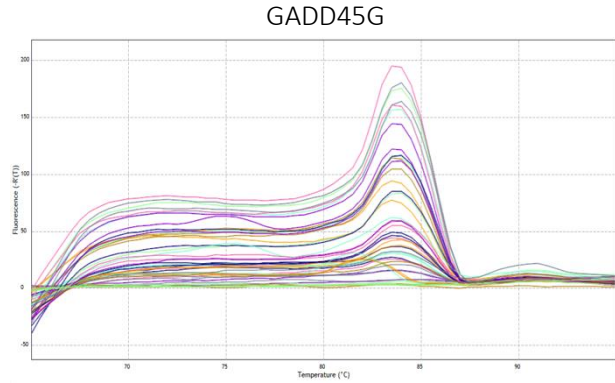
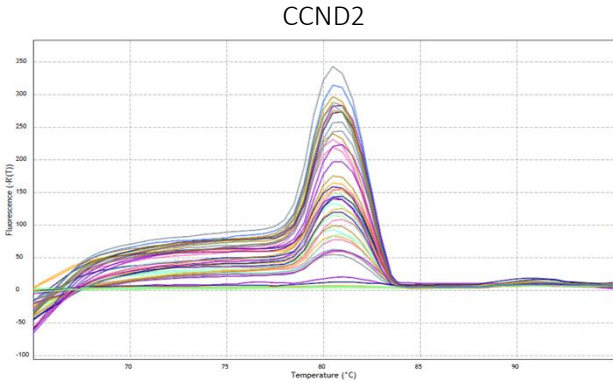
Standard curves:



Amplification curves:



Melt curves:



APPENDIX 3 – FLOW CYTOMETRY DATA OUTPUT

Side scatter (SSC) plotted against forward scatter (FSC) for the three GBM cell lines exposed to double-cycle treatment with TMZ and DMSO.

